Hillslope-glacier coupling: The interplay of topography and glacial dynamics in High Asia

Dirk Scherler,[1] Bodo Bookhagen,[2] and Manfred R. Strecker[1]

[1]   High Asian glacial landscapes have large variations in topographic relief and the size and steepness of snow accumulation areas. Associated differences in glacial cover and dynamics allow a first-order determination of the dominant processes shaping these landscapes. Here we provide a regional synthesis of the topography and flow characteristics of 287 glaciers across High Asia using digital elevation analysis and remotely sensed glacier surface velocities. Glaciers situated in low-relief areas on the Tibetan Plateau are mainly nourished by direct snowfall, have little or no debris cover, and have a relatively symmetrical distribution of velocities along their length. In contrast, avalanche-fed glaciers with steep accumulation areas, which occur at the deeply incised edges of the Tibetan Plateau, are heavily covered with supraglacial debris, and flow velocities are highest along short segments near their headwalls but greatly reduced along their debris-mantled lower parts. The downstream distribution of flow velocities suggests that the glacial erosion potential is progressively shifted upstream as accumulation areas get steeper and hillslope debris fluxes increase. Our data suggest that the coupling of hillslopes and glacial dynamics increases with topographic steepness and debris cover. The melt-lowering effect of thick debris cover allows the existence of glaciers even when they are located entirely below the snow line. However, slow velocities limit the erosion potential of such glaciers, and their main landscape-shaping contribution may simply be the evacuation of debris from the base of glacial headwalls, which inhibits the formation of scree slopes and thereby allows ongoing headwall retreat by periglacial hillslope processes. We propose a conceptual model in which glacially influenced plateau margins evolve from low-relief to high-relief landscapes with distinctive contributions of hillslope processes and glaciers to relief production and decay.

1.   Introduction

[2]   The idea that the topographic growth of glaciated mountain ranges may be limited by the erosive work of glaciers has gained much support in recent years [e.g., *Spotila et al.*, 2004; *Mitchell and Montgomery*, 2006; *Brocklehurst and Whipple*, 2007; *Berger and Spotila*, 2008; *Egholm et al.*, 2009]. Although the so-called "glacial buzz saw" mechanism was first proposed for the NW Himalaya where shallow slope angles and surface areas are concentrated near the long-term mean position of the snow line [*Brozović et al.*, 1997], unequivocal evidence from this region for highly erosive glaciers is rare. Low erosion rates on the NW Himalayan Deosai Plateau, for example, question the efficacy of glacial erosion in high-elevation low-relief areas [*van der Beek et al.*, 2009]. Whereas some authors expect only limited

glacial activity in the central Himalaya, due to high-altitude aridity and reduced ice flux [*Harper and Humphrey*, 2003], others suggest that in the long term, glaciers are as erosive as rivers at the monsoon-soaked Himalayan front [*Burbank et al.*, 2003; *Gabet et al.*, 2008].

[3]   The picture of glaciers sawing off topography at or near the snow line is too simplistic [*Anderson*, 2005], and does not explain observed relief differences in glacial landscapes [*Brocklehurst and Whipple*, 2007; *Pedersen et al.*, 2010]. Moreover, several studies have noted that headwall retreat can outpace glacial downcutting [*Oskin and Burbank*, 2005; *Naylor and Gabet*, 2007], which is difficult to reconcile with sliding-based glacial erosion laws, and points at an important contribution of periglacial hillslope processes to the shaping of glacial landscapes [e.g., *Hales and Roering*, 2005, 2007; *Heimsath and McGlynn*, 2008; *MacGregor et al.*, 2009]. In analogy to the coupling of hillslope and channel processes in fluvial systems, we ask ourselves if and how glacial and periglacial processes interact? Are these systems coupled and are there feedbacks and thresholds at which certain processes dominate?

[4]   The hillslope legacies of glacial systems are moraines and the debris on and in the glaciers. Material that is eroded

[1]Institut für Geowissenschaften, Universität Potsdam, Potsdam, Germany.
[2]Department of Geography, University of California, Santa Barbara, California, USA.

from glacial headwalls in the accumulation zone ultimately lands on the glaciers below, where it forms supraglacial debris once it is exposed in the ablation zone [e.g., *Boulton and Eyles*, 1979; *Hewitt*, 2009]. At debris thicknesses of <~2 cm, the lower albedo of debris compared to clean ice absorbs more incoming radiation energy and thus increases melt rates. In contrast, the insulating effect of debris cover dominates at thicknesses >~2 cm and melt rates decrease to values below those of clean ice [e.g., *Østrem*, 1959; *Mattson et al.*, 1993; *Kayastha et al.*, 2000]. Because debris cover strongly modulates melt rates [e.g., *Ogilvie*, 1904; *Østrem*, 1959] it also influences glacial mass balances and thus the size and geometry of glaciers. Based on these arguments, debris cover should therefore also have an effect on the magnitude and distribution of glacial velocities, which are first-order factors controlling their erosion potential.

[5] In a previous study, we observed many debris-covered Himalayan glaciers that respond to recent climate change by developing stagnating reaches in the last several km before their termini [*Scherler et al.*, 2011]. This is most likely due to lower melt rates beneath thick debris cover, which retards the response of debris-covered glaciers to climate change [cf. *Jóhannesson et al.*, 1989, equation (12)], and which commonly results in a distinctive form of glacier melting dominated by thinning instead of retreat [*Ogilvie*, 1904; *Clayton*, 1964; *Kirkbride*, 1993]. However, only glaciers situated in high-relief areas were found to carry significant amounts of debris. We therefore hypothesize that debris cover increases with topographic steepness because of enhanced mass wasting in steep accumulation areas.

[6] In this study, we focus on the coupling between ice-free hillslopes above glaciers, which are the sources for supraglacial debris, and the distribution and magnitude of glacial velocities. We conducted a large-scale regional survey at high spatial resolution of 287 glaciers in contrasting glacial landscapes of High Asia (Hindu Kush, Karakoram, Himalaya, Tibet) (Figure 1). We present analyses of glacial topographic characteristics, including a proxy for snow and ice avalanching, and mean glacier-surface velocities between 2000 and 2008 as an indicator for glacial erosion potential. We discuss our data with respect to geomorphic processes in high mountain environments and propose a conceptual model of glacial landscape development on plateau margins, which emphasizes the coupling between glaciers and hillslopes.

2. Study Area

2.1. Climatic Setting

[7] High Asia encompasses an extensive region of high elevations influenced by different atmospheric circulation systems (Figure 1). The center of this region is the Tibetan Plateau, at mean elevations of ~5 km above sea level (asl), which forms an important orographic obstacle for the midlatitude westerlies and the South and East Asian monsoons [*Hahn and Manabe*, 1975; *Benn and Owen*, 1998; *Boos and Kuang*, 2010]. In this study, we focus on regions along the southern, western, and northwestern margins of the Tibetan Plateau (Figure 1).

[8] Glaciers in the central Himalaya are dominated by a monsoonal climate, with a distinct accumulation season during summer (June to September) and a dry season in winter [*Ageta and Higuchi*, 1984]. Although monsoon pre-cipitation can reach very high amounts over the Himalaya [*Bookhagen and Burbank*, 2006; *Anders et al.*, 2006], most moisture is orographically forced out at elevations <4 km asl, and the high ice-covered parts of the orogen are significantly more arid [*Harper and Humphrey*, 2003].

[9] From east to west along the Himalaya, monsoon influence decreases and moisture supply by the midlatitude westerlies becomes more important. Notably, the moisture boundary lies at 78°E near the Sutlej Valley, where eastern regions receive most precipitation during summer and western regions receive most precipitation during winter [*Bookhagen and Burbank*, 2010]. Westerly derived precipitation is highest in winter and early spring when low-pressure systems known as Western Disturbances encounter the western margin of High Asia [*Barry and Chorley*, 2003]. The westerlies transport atmospheric moisture far into the orogen, which may be related to the higher tropospheric extent of the westerly airflow that helps to overcome orographic barriers. In these regions, annual precipitation of up to 2 m of snow water equivalent at high elevations where glaciers occur has been observed [*Winiger et al.*, 2005; *Wulf et al.*, 2010] or inferred from indirect methods [e.g., *Weiers*, 1994; *Bhutiyani*, 1999].

[10] At the northern rim of the Tibetan Plateau, the West Kunlun Shan is the most continental setting in our study area. In this region, limited precipitation is mainly derived from the East Asian monsoon during summer, resulting in glaciers confined to high elevations (Figure 1b) [*Ohata et al.*, 1989].

2.2. Present-Day Glaciation

[11] Currently, approximately 115,000 km^2 in central Asia are covered with glaciers [*Dyurgerov and Meier*, 2005]. Most of these areas are found along the margins of the Tibetan Plateau, and are characterized by steep topographic and climatic gradients (Figure 1). The areal extent of accumulation areas and thus the occurrence and size of glaciers mostly depends on gradients in topography and precipitation and the resulting changes in snow line elevation. Snow lines are high above the Tibetan Plateau (>5.5 km asl [*von Wissmann*, 1959; *Ohmura et al.*, 1992]) and only intersect locally with mountains that protrude usually not more than a kilometer above the surrounding areas. Toward the southern and western margins of the Tibetan Plateau, snow lines descend due to increasing amounts of precipitation [*Ohmura et al.*, 1992]. In the western Himalaya and Karakoram, snow line elevations are lower than farther east, most likely due to latitudinal temperature gradients and the influx of winter precipitation from the west [*von Wissmann*, 1959]. An important aspect of Himalayan glaciers is the outstanding role of snow and ice avalanches to snow accumulation [e.g., *Schlagintweit*, 1871; *von Wissmann*, 1959; *Inoue*, 1977; *Benn and Lehmkuhl*, 2000], and the high concentration of extensively debris-covered glaciers in this region [*Scherler et al.*, 2011].

3. Topography and Debris Cover

3.1. Methods

3.1.1. Glacier and Debris Cover Mapping and Topographic Analysis

[12] We manually digitized the outlines of the 287 studied glaciers using orthorectified ASTER band 3N images with
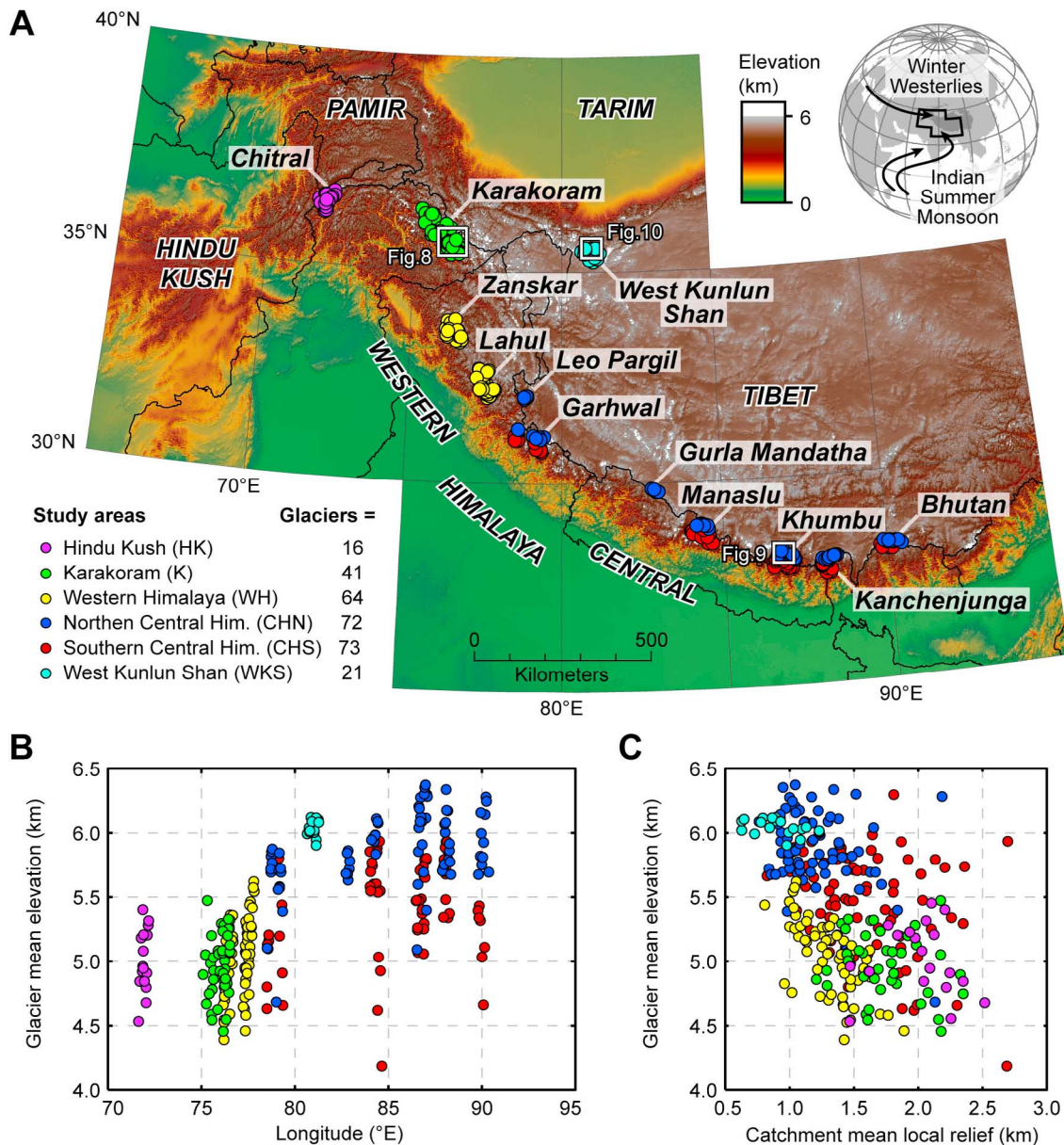
Figure 1. Geographic setting of the study areas in High Asia. (a) Digital elevation model of western Tibet and adjacent mountain ranges. Circles indicate the location of the analyzed glaciers, colored by region. Black lines mark international borders. Mean surface elevation of the studied glaciers versus (b) zonal position and (c) mean local relief calculated over a 5 km radius of their catchment.

15 m ground resolution in the near infrared (NIR) spectral range and Système Probatoire d'Observation de la Terre (SPOT) 4 and 5 panchromatic images with ground resolutions of 10 and 5 m, respectively (see Tables S1 and S2 in Text S1).[1] All images were acquired between the years 2000 and 2008. See section 4.1 for details on the orthorectification procedure. Glacier outlines from the Global Land Ice Measurements from Space (GLIMS) database [*Kargel et al.*, 2005] provided assistance during digitizing but could not be used exclusively, because many of the analyzed glaciers were not included, and several glacier outlines did not match the observed glacier extents. During digitizing, we followed the GLIMS analysis tutorial guidelines available at [http://www.glims.org/MapsAndDocs/guides.html].

[13] The manually defined glacier outlines include debris-free and debris-covered parts. We used orthorectified Landsat TM and ETM+ imagery acquired between 1990 and 2001 (see Table S3 in Text S1) with high snow lines and low snow cover, mostly from late summer and fall to map snow and ice covered areas from band TM4/TM5 ratios [e.g., *Paul et al.*, 2004]. Applying a threshold of 2.0 [*Paul et al.*, 2004] to the ratio images and blending the resulting binary images with the manually digitized glacier outlines allowed us to discriminate debris-free and debris-covered ice.
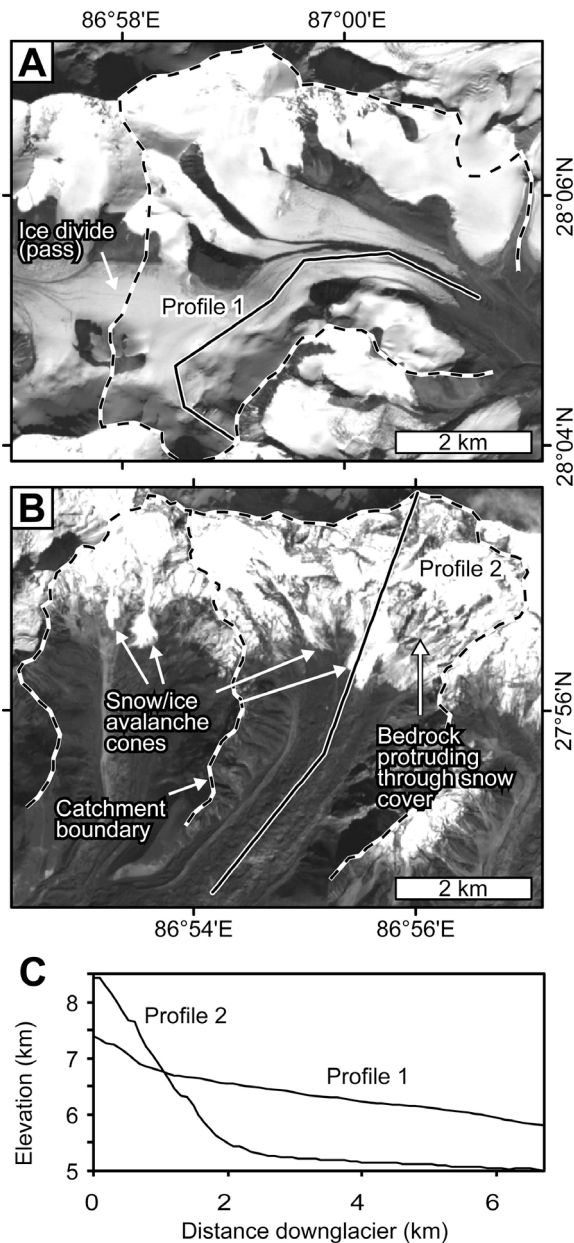
Figure 2. End-member examples of avalanche accumulation. Orthorectified ASTER images of glaciers with (a) low contribution of avalanches to accumulation and (b) high contribution of avalanches to accumulation. (c) Topographic profiles from each glacier. Examples in Figures 2a and 2b are located ~11 km north and ~7 km south of Mount Everest, respectively (Khumbu area; see Figure 1).

[14] We investigated the topography of the analyzed glaciers and corresponding catchments with a 90 m resolution digital elevation model (DEM), based on Shuttle Radar Topography Mission (SRTM) data [*Farr et al.*, 2007]. As the original SRTM-DEM contains significant holes without data in high-relief terrain [e.g., *Kääb*, 2005], we used an SRTM-based DEM, in which larger voids have been patched with digitized contours from topographic maps (J. de Ferranti, 3″ resolution digital elevation data for High Asia, 2007, http://

www.viewfinderpanoramas.org/dem3.html). We filled small remaining holes by bilinear interpolation. Because these holes are very small and mainly located outside of the studied catchments and glaciers they do not impact our results.

[15] Contributing areas above the glacier surfaces, i.e., catchment areas, were calculated using the DEM and the D8 flow-routing algorithm [*O'Callaghan and Mark*, 1984]. We manually checked all results for consistency. For analyzing catchment topography, we produced maps of local topographic relief by measuring the elevation range in a 5 km radius and surface slope within a 3×3 pixel moving window.

3.1.2. Snow Lines, Equilibrium Line Altitudes, and Accumulation Area Ratios

[16] Several simple methods exist for estimating the equilibrium line altitude (ELA) of glaciers [e.g., *Benn and Lehmkuhl*, 2000; *Osmaston*, 2005]. Most of these methods require a priori knowledge of, e.g., the accumulation area ratio (AAR) or mass balance profiles, which are unknown for the studied glaciers. Consequently, we obtained estimates of the snow line elevation using orthorectified satellite images (ASTER, SPOT, and Landsat) that were acquired near the end of the hydrological year (fall), when snow cover is lowest [e.g., *Rabatel et al.*, 2005]. We manually determined the surface elevation at the boundary between bright snow and darker ice from the DEM. The temporal coverage of the observation period with suitable scenes varies from region to region and only allows a rough estimate of the snow line. We estimate an uncertainty in our snow line elevations, based on the observed temporal and spatial variability of snow lines for each glacier. This approach is somewhat subjective and the relative discrepancies can vary, but provides a useful estimate in the absence of better data. On average ~20 images are available per region and most of them are from near the end of the hydrological year (see Table S1 in Text S1). We used the snow line estimates as a proxy for the transient ELA and to calculate AARs [*Meier and Post*, 1962; *Rabatel et al.*, 2005]. The approximated transient ELAs are most likely different from the zero-net mass balance steady state ELAs and their corresponding AARs. However, for the scope of our study, the snow lines or transient ELAs and derived AARs provide reasonable first-order estimates for the investigated time period [cf. *Meier and Post*, 1962].

3.1.3. Identifying Avalanche Accumulation

[17] Snow and ice avalanches are important processes contributing to snow accumulation on glaciers in high mountain environments [*Inoue*, 1977; *Benn and Lehmkuhl*, 2000]. Yet, quantitative data on snow avalanche size-frequency distributions, for example, are unavailable for the studied glaciers. Here, we use a simple proxy for the relative importance of avalanche accumulation, which we define by the extent of ice cover in the accumulation area: the higher the percentage of ice-free areas in the accumulation area of a given glacier, the higher the amount of snow-avalanche accumulation. This proxy acknowledges the fact that all areas above the snow line receive snowfall, but that the buildup of ice is only possible where hillslopes are gentle enough to retain the snow. Where hillslopes are too steep, the snow is transferred to lower elevations by avalanches. Two examples with end-member-type accumulation areas are shown in Figure 2. The two glaciers are only ~18 km apart, located north and south of Mount Everest, Nepal. The northern glacier has only a few patches of ice-free bedrock cropping out

Table 1. Regional Statistics of Selected Catchment and Glacier Properties[a]

	Geographic Region					
	HK	K	WH	CHS	CHN	WKS
Glacier Area as a Function of Catchment Area (y = ax)						
a	0.40 ± 0.05	0.50 ± 0.03	0.43 ± 0.02	0.37 ± 0.02	0.43 ± 0.03	0.73 ± 0.03
R^2	0.9	0.97	0.94	0.94	0.78	0.98
Mean Catchment Relief (km)						
Mean	2.0	1.7	1.3	1.6	1.2	0.9
Median	2.1	1.7	1.3	1.6	1.1	0.9
SD	0.3	0.3	0.2	0.4	0.3	0.2
Mean Glacier Slope (deg)						
Mean	21.2	18.8	15.4	17.5	15.8	12.8
Median	20.2	18.7	15.0	17.6	15.0	12.4
SD	3.2	3.4	2.9	3.5	4.1	4.3
Debris Cover (%)						
Mean	22.9	20.5	21.3	34.6	17.9	2.8
Median	23.0	19.8	15.9	30.0	12.6	2.2
SD	10.3	12.8	16.3	22.8	16.0	2.2
Accumulation Area Ratio (AAR)						
Mean	0.46	0.58	0.48	0.42	0.60	0.80
Median	0.45	0.62	0.53	0.47	0.63	0.81
SD	0.09	0.16	0.21	0.26	0.18	0.07

[a]Geographic regions are the high Hindu Kush (HK), Karakoram (K), western Himalaya (WH), southern central Himalaya (CHS), northern central Himalaya (CHN), and West Kunlun Shan (WKS). The uncertainties for factor *a* in the catchment area glacier area relationship correspond to the 90% confidence intervals; all other standard deviations (SD) refer to 1-sigma intervals.

in its accumulation area and therefore must receive most snow by direct snowfall on the glacier surface. In contrast, the accumulation area of the southern glacier is much steeper, hence mostly ice free, and avalanche cones on the glacier surface next to the base of the headwalls provide evidence for recent snow avalanches.

3.2. Results
3.2.1. Regional Differences in the Topographic Setting
[18] We collected data in 12 different regions ranging from the high Hindu Kush to the eastern central Himalaya (Figure 1) and grouped these regions into six greater geographic regions, based on similarities in climate and topography [*Scherler et al.*, 2011]. From west to east, following decreasing influences of the westerlies and increasing influences of the Asian monsoons, these are (1) the high Hindu Kush (HK), (2) Karakoram (K), (3) western Himalaya (WH), (4) West Kunlun Shan (WKS), and (5) central Himalaya (CH). In the central Himalaya, we further distinguish between glaciers that are situated south (CHS) or north (CHN) of the main topographic divide between the Himalaya and the Tibetan Plateau.

[19] The surfaces of glaciers in the Hindu Kush, Karakoram, and western Himalaya have similar mean elevations and are usually lower than glaciers in the central Himalaya and West Kunlun Shan (Figure 1b). The mean surface elevations of northern central Himalayan glaciers are on average ~6.0 km asl, whereas those of southern glaciers are on average ~5.0–5.5 km asl, with a larger elevation range. Differences in mean elevation are partly accompanied by differences in mean local relief of the corresponding catchments (Figure 1c). Mean local relief is lowest for the analyzed catchments in the West Kunlun Shan and in the northern central Himalaya, but it is significantly higher for catchments in the Hindu Kush, Karakoram, and the southern

central Himalaya. The western Himalaya takes an intermediate position.

[20] Regional variations in catchment relief are also reflected in the mean slope values of the associated glaciers (Table 1). The average ratio of glacier areas with respect to their catchment areas (including glaciers and snowfields that are not connected with the studied glaciers), is ~40% and similar in most regions except for the Karakoram, where it is ~50%, and the West Kunlun Shan, where it is ~73% (Table 1).

3.2.2. Variations in Debris-Covered Areas and Avalanche Accumulation
[21] Glaciers with significant debris cover (>12%) exist in all regions except for the West Kunlun Shan, where the mean debris-covered area is <3% (Table 1). The highest mean value and variability (1σ) in debris-covered areas is found for glaciers from the southern central Himalaya ($34.6 \pm 22.8\%$), whereas in the northern part of the central Himalaya, debris-covered areas are lower ($21.3 \pm 16.3\%$).

[22] Glaciers with high percentages of debris cover have high percentages of ice-free areas above the snow line, i.e., in the accumulation areas, which we use as a proxy for the relative importance of snow avalanche accumulation (Figure 3). The catchments and glaciers with large inferred amounts of avalanche accumulation have lower hypsometric integrals (HI) compared to glaciers that are dominantly fed by direct snowfall (Figure 3b). The HI measures the distribution of planimetric area with respect to elevation; a low (high) value indicates that the bulk of area is found at lower (higher) elevations. In consequence, the median (and mean) elevation of glaciers with large inferred amounts of avalanche accumulation is often located far below the approximate elevation of the snow line that we obtained from the satellite images (Figure 3c). This confirms theoretical expectations [*Benn and Lehmkuhl*, 2000]. A corollary is that glaciers with large
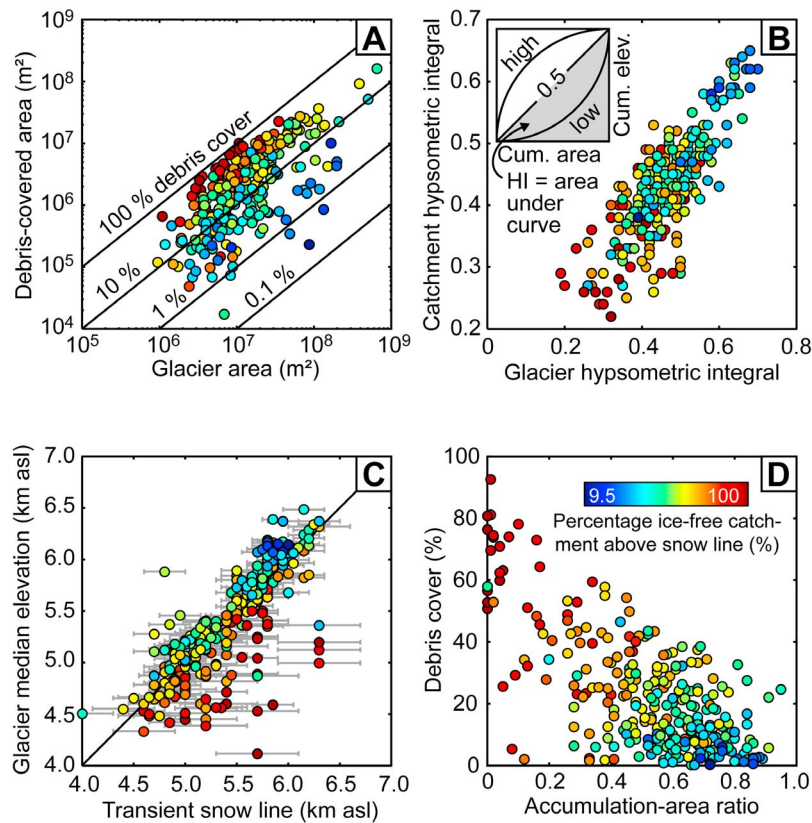
Figure 3. Topographic characteristics of avalanche accumulation glaciers. Marker colors depict degree of avalanche accumulation approximated by the percentage of ice-free catchment areas above the snow line (see text for details). (a) Glacier area versus debris-covered area. (b) Glacier hypsometric integral versus catchment hypsometric integral. Avalanche-fed glaciers and their catchments have areas skewed to lower elevations. (c) Transient snow line (2000–2008), estimated from satellite images versus glacier median elevation. Avalanche-fed glaciers typically have most areas below the snow line. (d) Accumulation area ratio (AAR) versus debris-covered area.

inferred amounts of avalanche accumulation have low AARs and vice versa, although there are also glaciers with low inferred amounts of avalanche accumulation and a low AAR (Figure 3d).

[23] It previously has been shown that debris-covered glaciers in the Himalaya have steep accumulation areas, including ice-free and ice-covered areas, with mean slope angles >25° [*Scherler et al.*, 2011]. Here, we test if this trend aligns with our proxy for snow and ice avalanching (Figure 4). When mean slope angles of ice-free areas above the snow line (the source areas for snow and ice avalanches) exceed 25°, the percentages of both, debris cover and ice-free catchment areas, increase quite abruptly but show large scatter (Figure 4a). Although avalanching is restricted to ice-free hillslopes, their abundance with respect to the glacier area is equally important. The percentage of debris cover and ice-free catchment areas increase somewhat more gradual with mean slope angles of all catchment areas above the snow line because of the inclusion of ice-covered areas: if ice-free areas above the snow line are relatively small, the generally less steep glacier areas dominate the mean slope angle. Therefore, particularly those glaciers with small ice-free areas and low debris cover are shifted to lower mean slopes in Figure 4b. The increases of debris cover with mean slope angles above

the snow line is best depicted by a power law ($y = 2.5e-4 \pm 1.8e-4 * x^{3.34 \pm 0.37}$, $R^2 = 0.52$).

4. Glacier Surface Velocities

4.1. Methods

[24] We obtained glacier surface velocities from sub-pixel correlation of orthorectified ASTER and SPOT images in the frequency domain using the freely available software COSI-Corr [*Leprince et al.*, 2007, 2008] and following the methodology described by *Scherler et al.* [2008]. In short, two scenes taken at different times are orthorectified using the SRTM-based DEM, coregistered and correlated, and the subpixel displacement of features on the glacier surface is recorded at every 4th pixel in the 15 m resolution orthorectified ASTER images, providing measurements of the horizontal surface velocity for every 60 m. We used multiscale window sizes of 128 × 128 down to 32 × 32 pixels, thus effectively smoothing the measured velocities over 2-D Hanning windows of 31 × 31 pixels [*Leprince et al.*, 2007]. For similar procedures, see, for example, *Scambos et al.* [1992], *Kääb* [2005], and *Berthier et al.* [2005].

[25] Residual uncertainties in the displacement measurements, i.e., after correcting for distortions related to attitude
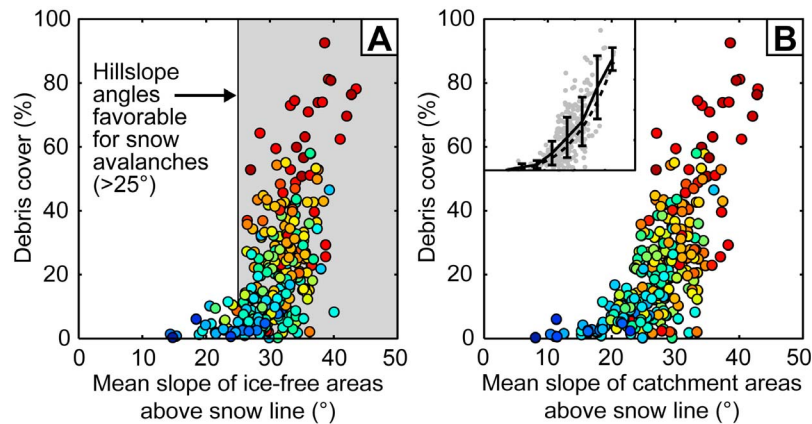
Figure 4. Relationship between steepness of accumulation areas and percentage of debris-covered areas. (a) Mean slope of ice-free areas above snow line. Note the sharp increase of debris-covered areas at mean slope angles >25°. Hillslope angles favorable for snow avalanching after *Luckman* [1977]. (b) Mean slope of catchment area (including ice-covered and ice-free areas) above the snow line. Inset shows mean and standard deviation of debris cover in 5° mean slope bins (solid black line) and a power law fit (dashed black line; see text for details). Color scale of markers gives percentage of ice-free catchment above the snow line (see Figure 3).

variations, are on the order of 2–4 m per correlation and mainly related to inaccuracies in the DEM used for orthorectification and noise in the correlation results [*Avouac et al.*, 2006; *Scherler et al.*, 2008]. These uncertainties get smaller (larger) for images separated by more (less) than a year (see Table S4 in Text S1). For the purpose of our study, however, the degree of data coverage for each glacier is more important than the subpixel accuracies achieved with COSI-Corr. On average, we used ~20 orthorectified images per study region and ~20–30 image correlations with velocity measurements per glacier (see Table S4 in Text S1). For some of the studied glaciers we have only few correlations available, but we decided to retain them in our sample when the velocity data show only minor scatter. Most of the image pairs we used in this study are separated by one or several years. In parts of some fast flowing glaciers, it proved useful to correlate imagery separated by a few months, because rapid surface changes cause the correlation to fail.

[26] For the purpose of data comparison, we measured the surface velocity along a manually identified central flow line of each of the 287 glaciers. This reduces the data complexity and also facilitates comparing a large number of glaciers of different sizes. In the case of complex branching glaciers, we selected the main valley glacier and did not consider multiple profiles along the tributary glaciers. The profile points are spaced at 60 m, and on average ~10 velocity measurements from different velocity maps and years were available per point. In order to reduce the number of miscorrelations in the velocity profiles, we filtered the velocity data by direction and magnitude [*Scherler et al.*, 2008].

[27] In our previous study [*Scherler et al.*, 2011], we focused on the slow moving lower parts of the glaciers where image cross correlation is straightforward and data coverage generally good. In this study, we are interested in continuous velocity profiles that cover the entire length of the glaciers. This may pose problems in some areas. Data coverage is generally poorer in areas (1) of featureless glacier surfaces, as for example in some low-gradient accumulation areas, and (2) where rapid changes of the glacier surface complicate

feature tracking, such as reaches where a glacier flows over steep bedrock or in the depositional areas of snow avalanches [*Scherler et al.*, 2008]. In these areas, uncertainties in the velocity measurements are generally higher. A continuous velocity profile was generated for each glacier by computing the average velocity for each profile point and linear interpolation at profile points with no measurements. The studied glaciers, ranging in length from 2 to 66 km, have mean data gap sizes of 1.3% ($\pm 1.6\%$, 1σ) of their profile lengths. To eliminate the influence of spurious outliers at portions of low data coverage, final velocities are obtained by smoothing the velocity profiles with a five-point moving average filter.

[28] We characterized the horizontal distribution of velocities for each glacier by (1) determining the position of the peak velocity along the glaciers and (2) computing the ratio of the mean velocity measured in the upper versus the lower half of the glacier. We also computed a mean velocity for each glacier by averaging over the entire velocity profile. Because the velocity profiles of some of the glaciers contain data gaps in crucial positions, we excluded a total number of 33 glaciers from either one or both of these analyses. This number includes three glaciers from the West Kunlun Shan, which have unusually low velocities at their frontal parts most likely associated with past surges. Distorted medial moraines at seven of the studied Karakoram glaciers and one glacier from the Hindu Kush suggest surging behavior of tributary glaciers [e.g., *Hewitt*, 2007], but we retained these glaciers in our analysis. Figures and tables with details on all studied glaciers, their velocity profiles, and the criteria for excluding certain glaciers from the more detailed analysis are provided in the auxiliary material (Figure S1 and Tables S5–S8 in Text S1).

4.2. Results

4.2.1. Regional Distribution of Glacier Surface Velocities

[29] Across the entire study area, we measured the highest glacier surface velocities in the Karakoram, where most velocities are >20–40 m/yr (Figure 5). Several of the largest
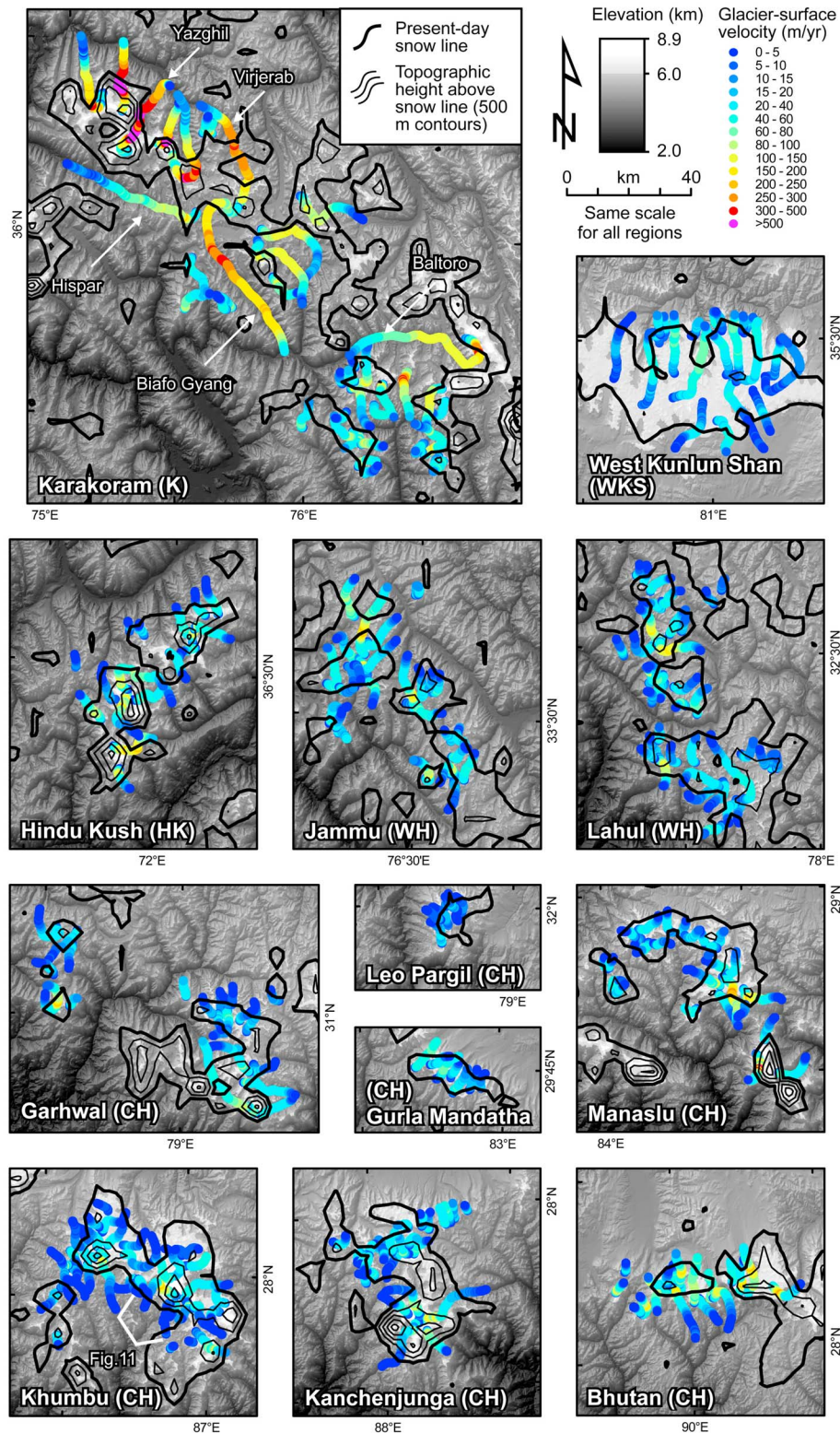
Figure 5. Regional patterns of glacier surface velocities. See Figure 1 for regional setting of study areas. Only surface velocities following the central flow line of the studied glaciers are shown, and only those glaciers with sufficient data are used to construct velocity profiles covering the entire glacier. For each glacier we picked only one velocity profile to prevent overlap. Thus, the number of studied glaciers in the Karakoram is relatively low with respect to the much greater ice-covered areas. Present-day regional climatic snow lines after *von Wissmann* [1959]. This data set comprises contour lines that were digitized and interpolated on a coarse (5 km resolution) grid. Note that the snow lines are likely too high in the Karakoram and too low in the southern central Himalaya.
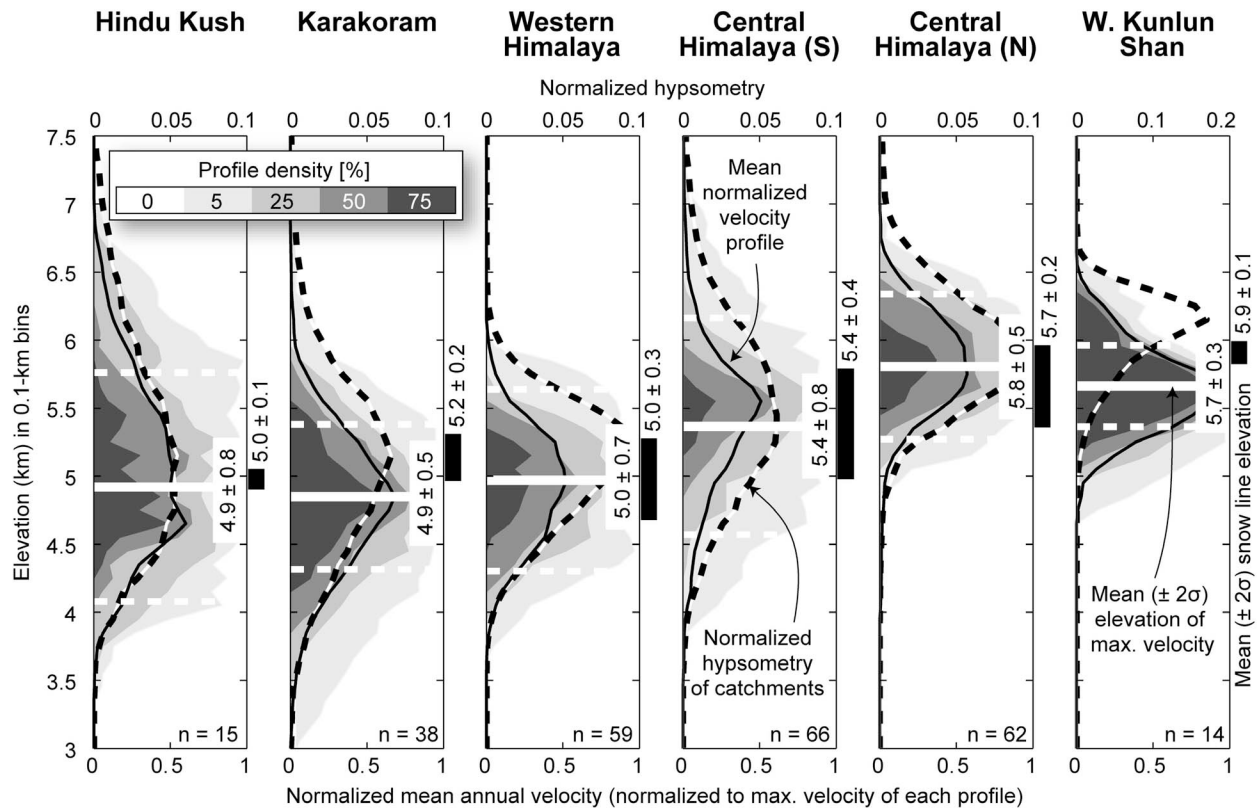
Figure 6. Altitudinal distribution of normalized glacier surface velocities in the six geographic regions. Profile density is defined as the percentage of profiles exceeding certain normalized velocities within 0.1 km elevation bins. Hypsometry of catchments is regionally aggregated. White horizontal bold and dashed lines indicate mean ($\pm 2\sigma$) elevation of maximum velocity. Black bars right of the velocity plots indicate the mean ($\pm 2\sigma$) elevation of satellite-derived snow line estimates. Note that several glaciers have been excluded from this plot due to data gaps in crucial positions (see Table S8 in Text S1).

glaciers (>20–30 km length), such as Baltoro, Biafo, Yazghil, and Virjerab, flow with velocities >100 m/yr over much of their length, and attain peak velocities of up to 1000 m/yr along steep segments. In all other study areas, most of the velocities are ≤20–40 m/yr, whereas velocities >100 m/yr are only found at steep segments of long glaciers (>15 km length). However, glaciers with accumulation areas that are too steep to allow ice build up, such as several south flowing glaciers in the southern central Himalaya, have low gradients over much of their course and any steep portion along the flow path is either absent or confined to short (<5 km) horizontal distances near the headwalls. These glaciers have the highest velocities at their far upstream end, but velocities quickly diminish downstream.

[30] In general, the fastest glaciers in each region are associated with the highest topography where the largest accumulation areas are located. In the West Kunlun Shan, where topography and relief are more subdued, large interconnected accumulation areas exist, but flow velocities are relatively low and local velocity peaks are absent. The spacing of contour lines in Figure 5 indicates that particularly steep accumulation areas exist in the southern central Himalaya, the Hindu Kush, and in the northwestern part of the Karakoram, whereas accumulation areas are less steep in the western Himalaya, the northern central Himalaya, and the central and southeastern part of the Karakoram.

[31] Figure 6 shows normalized velocity profiles plotted against elevation and grouped by region. The profile densities indicate the altitudinal distributions of glacier surface velocities within each region and show that glaciers flow fastest in an elevation band of ~1–1.5 km vertical extent, approximately centered on the hypsometric maximum of the (ice-covered) catchments (Figure 6). This band is lowest in the westerlies-influenced Hindu Kush, Karakoram, and western Himalaya at ~4.9–5.0 ± 0.8 km asl ($\pm 2\sigma$). In the monsoon-dominated central Himalaya it is located at ~5.4 ± 0.8 km asl to the south, and rises to 5.8 ± 0.5 km asl north of the Himalayan crest and is similarly high in the West Kunlun Shan. Generally, velocities are highest near the snow line, which is in accordance with theoretical expectations of glacier flow [e.g., *Anderson et al.*, 2006].

[32] In summary, glacier surface velocities across the study area appear to show first-order regional differences in total magnitude and the relative distribution along the length of the glaciers. In sections 4.2.2, 4.2.3, and 4.2.4, we present glacier velocities from three key regions, the central Karakoram, the Khumbu Himal in the central Himalaya, and the West Kunlun Shan, to explore the controlling factors and highlight regional contrasts. We selected these regions due to their marked differences in topographic and climatic setting (Figures 1 and 7), and show details from two glaciers per region, which point out details and characteristic features in the
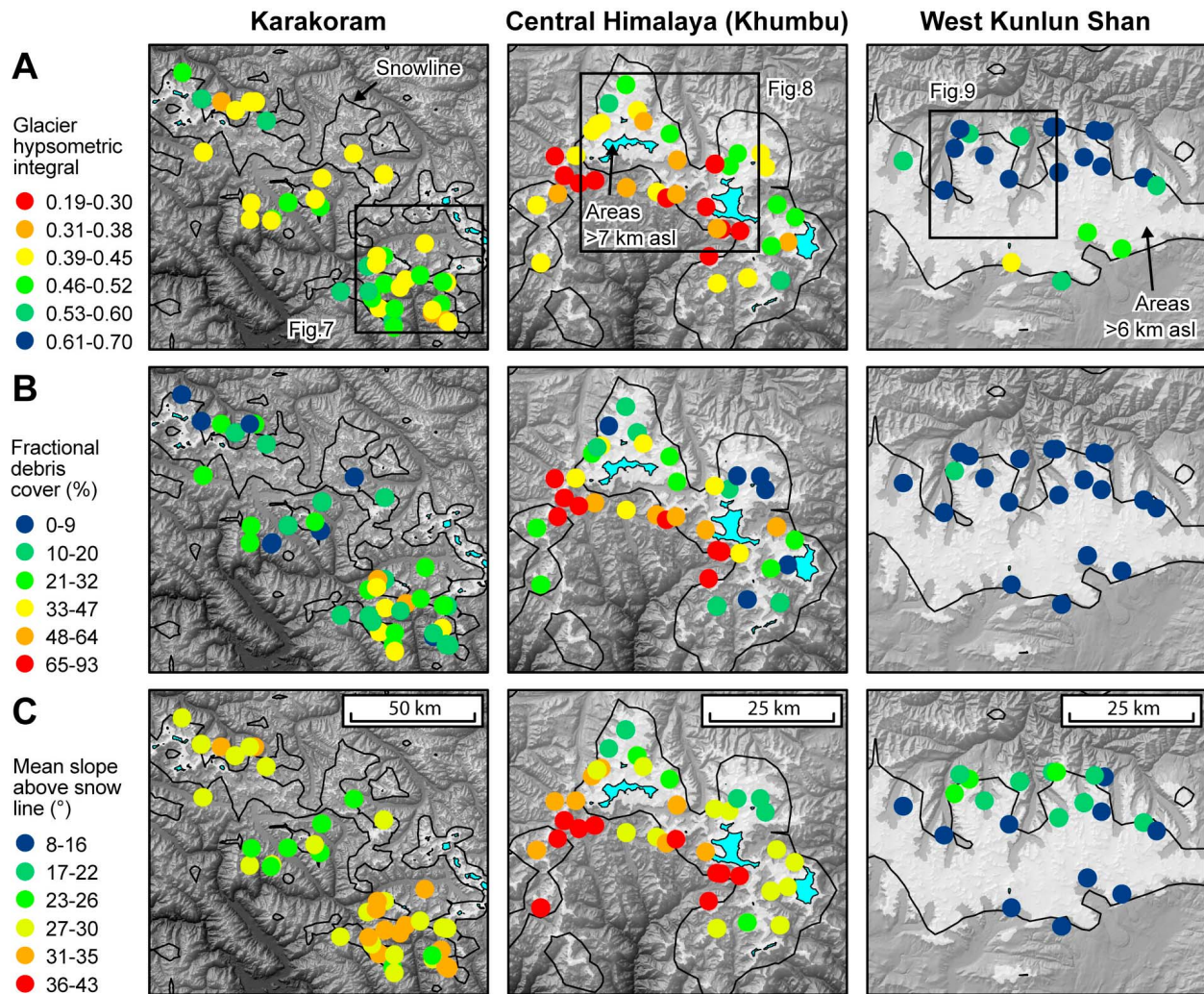
Figure 7. Topographic characteristics of the three case study regions: Karakoram (K), Khumbu Himal in the central Himalaya (CHS), and west Kunlun Shan (WKS). Each point represents a glacier and is plotted at the center position of a glacier-bounding rectangle. (a) Glacier hypsometric integral (HI). High HIs indicate glaciers in plateau-like landscapes with wide and shallow accumulation basins, whereas low HIs indicate glaciers in dissected landscapes with steep headwalls and high relief. (b) Percentage of debris-covered areas. (c) Mean slope of glacier and catchment areas above snow line. Black line indicates present-day regional climatic snow line after *von Wissmann* [1959].

glacier surface velocities that are widespread among many other glaciers (see Figure S1).

4.2.2. Case Study 1: Central Karakoram

[33] With >16,600 km² of glacial cover, the Karakoram is the most heavily ice-covered region in High Asia [*Dyurgerov and Meier*, 2005]. In the central and northwestern part, the glaciers are generally larger and interconnected, limiting the number of individual, nonoverlapping velocity profiles. Shorter glaciers with suitable data coverage were mostly found in the southeastern part of the Karakoram, south of Baltoro Glacier (Figure 7). On average, the glaciers have AARs of 0.58 ± 0.16 (1σ), and $20 \pm 13\%$ of their surface area is covered with debris. Mean catchment relief is 1.7 ± 0.3 km and the glaciers have mean slopes of $19 \pm 3°$. Most of the glaciers have relatively large firn fields at high elevations, but flow down into deeply incised valleys with steep hillslopes.

[34] The 60 km long Baltoro Glacier and the 14 km long Masherbrum Glacier (Figures 8c and 8d) both attain peak velocities of almost 400 m/yr locally. Velocities are usually low in the uppermost accumulation basins, but quickly increase within steeper reaches along the flow path. Particularly the large glaciers with multiple tributaries eventually reach a point of reduced steepness, after which velocities are much lower and decrease steadily toward the glacier's terminus with less variability in surface slope and velocity. Where major tributaries join the ice stream, flow velocities often increase by up to ~50%, unless the joining glacier does not contribute any significant ice discharge. The two main branches of the upper part of Baltoro Glacier, for example, meet at the confluence known as Concordia (Figure 8a) and the surface velocities increase by ~40–50% over a distance of 3 km. In contrast, the joining of smaller tributary glaciers downstream of Concordia results in only subtle velocity variations.
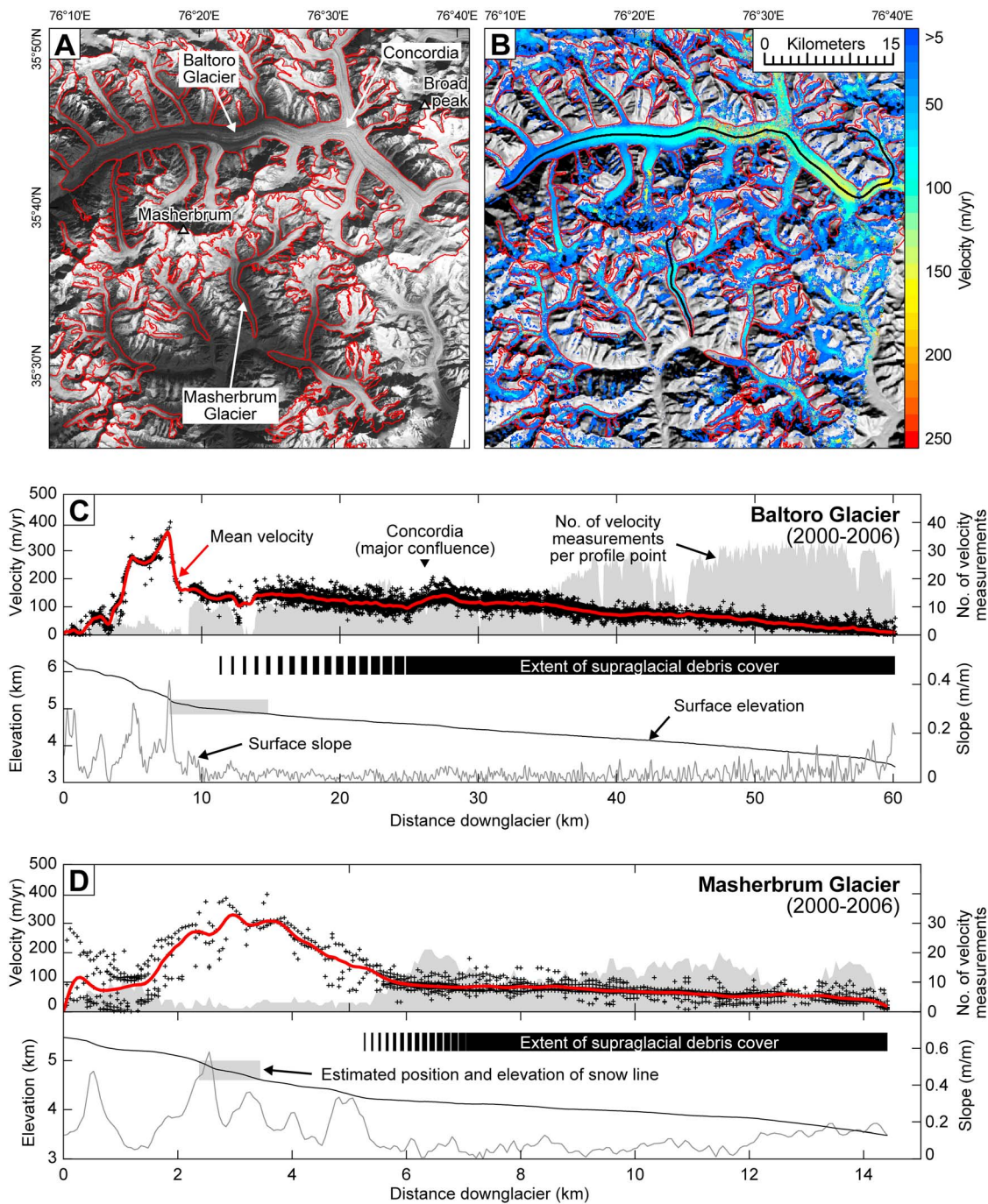
Figure 8. Case studies from the central Karakoram. (a) Orthorectified ASTER satellite image from October 2003. Red polygons delineate the studied glaciers. (b) Velocity map derived from correlation of the image in Figure 8a with another image from October 2002. Only velocities >5 m/yr are shown. The black lines show the trace of the profiles in Figures 8c and 8d. (c) Velocity, surface elevation, and along-profile surface slope of Baltoro Glacier. Black crosses are the available velocity measurements after filtering. Red line depicts the mean annual velocity, derived from averaging the velocity measurements at each profile point, interpolating over no-data profile points and smoothing with a five-point running average filter. Concordia is the place where the northern and southern branches of Baltoro Glacier meet (see Figure 8b). (d) Same as Figure 8c but for Masherbrum Glacier.

[35] Apart from some random residual miscorrelations, we observe considerable variations in the velocity data along certain segments of the velocity profiles (Figure 8). Whereas some scatter in the steep, upper parts of the glaciers is due to cross-correlation difficulties, we also observe systematic interannual velocity variations of ~50 m/y in the slower moving, lower parts of the glaciers. *Quincey et al.* [2009b] reported interannual velocity variations of Baltoro
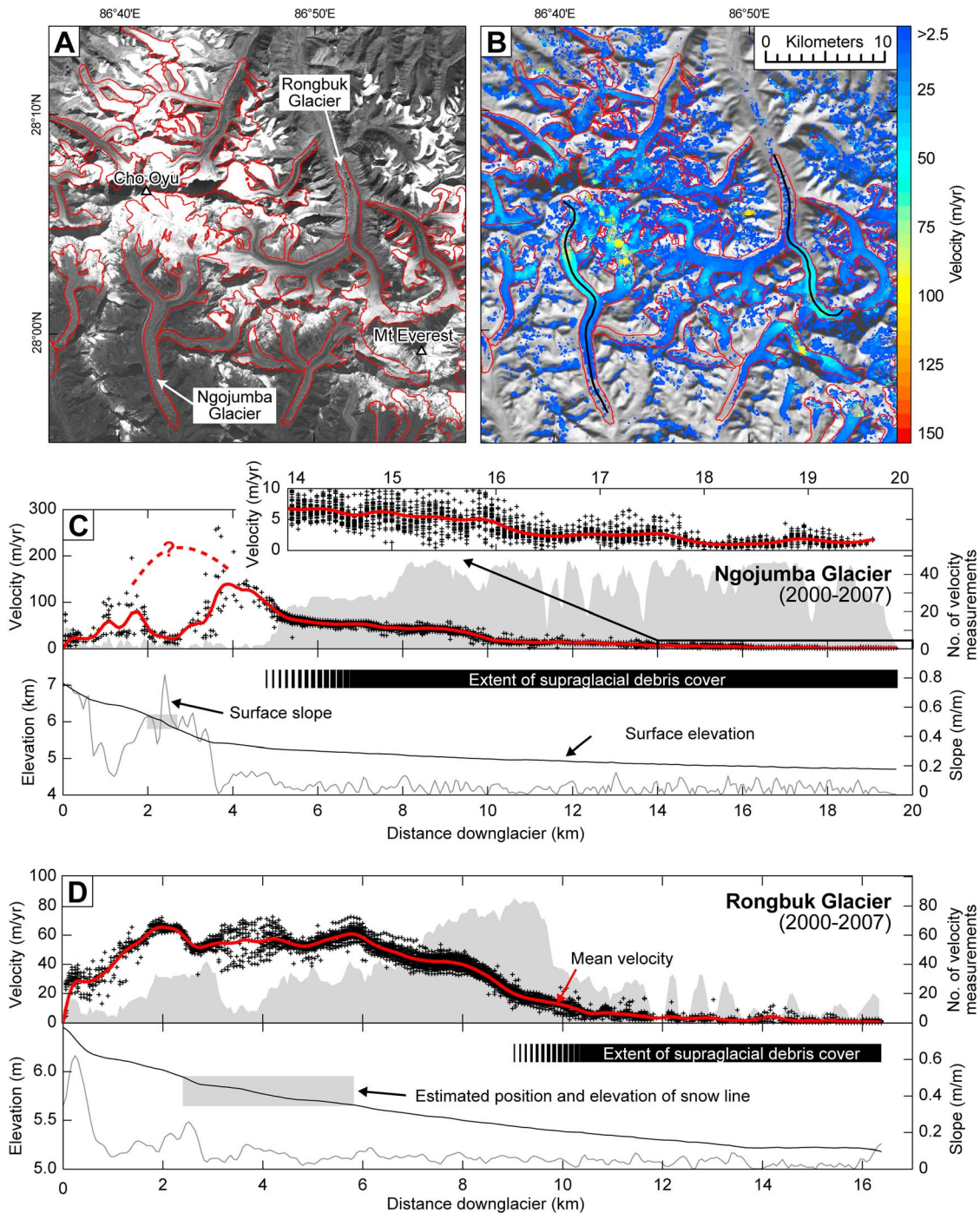
Figure 9. (a-d) Case studies from Khumbu Himal in the central Himalaya. Symbols are the same as in Figure 8. The orthorectified image in Figure 9a is a mosaic from two images acquired in November 2004. The velocity map in Figure 9b is also a mosaic and was produced by correlation of the image in Figure 9a with another image from November 2005 and from correlation of images acquired in October 2003 and 2004. Inset in Figure 9c has the *y* axis on the right and depicts velocities over the lower ~5–6 km of Ngojumba Glacier. Note changes in the *y* axis scaling from Figure 9c to Figure 9d.

Glacier between 1993 and 2008 that are of similar magnitude as in our study and not related to seasonal velocity fluctuations. We observe significant interannual velocity variations at other glaciers from the Karakoram (see Figure S1), but so far, we did not quantify their regional significance.

4.2.3. Case Study 2: Khumbu Himal (Central Himalaya)

[36] The Khumbu Himal is a horseshoe-shaped region of high topography in the central Himalaya of eastern Nepal, with Mount Everest (8848 m asl) located on the topographic
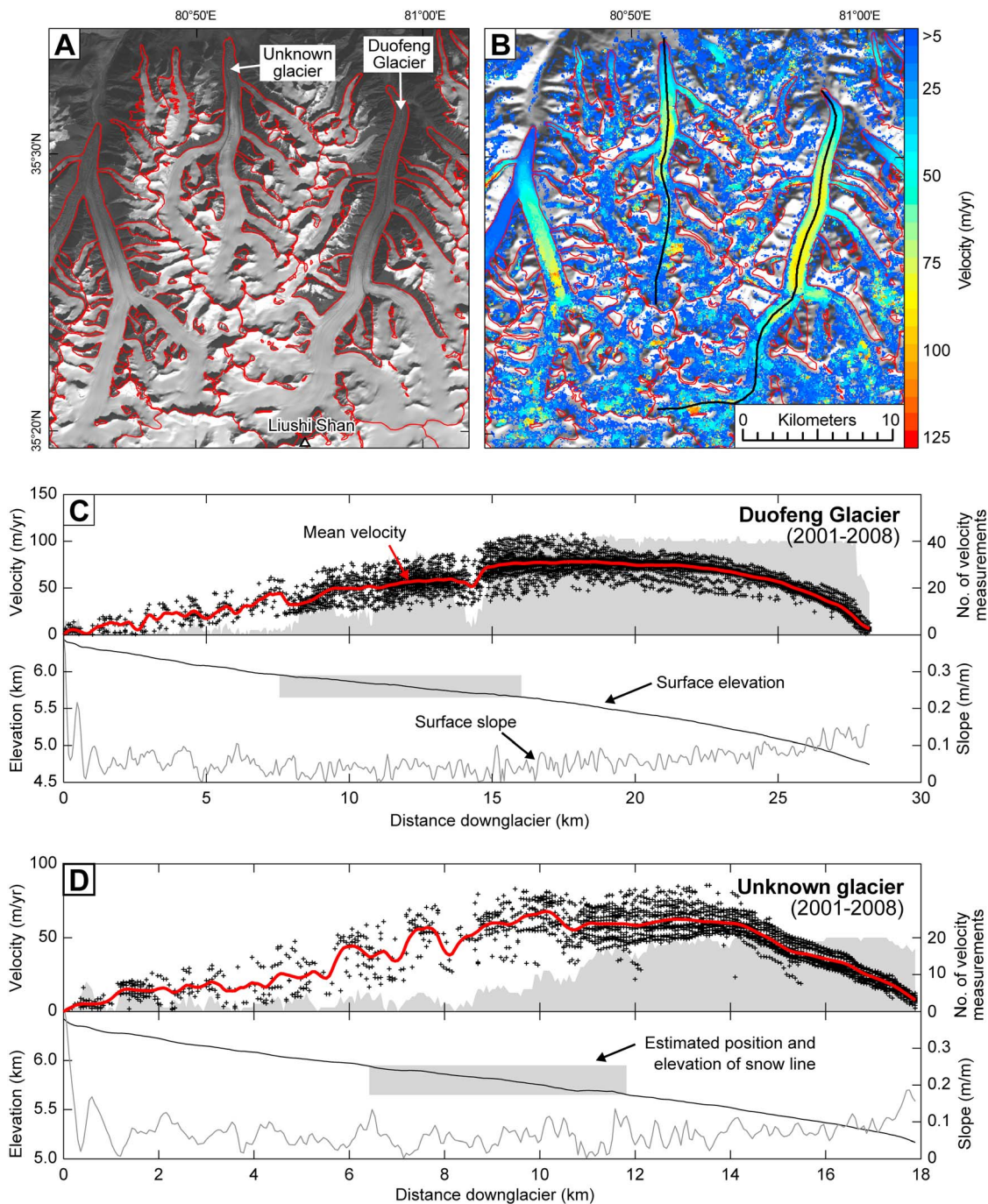
Figure 10. (a-d) Case studies from the West Kunlun Shan. Symbols are the same as in Figure 8. The orthorectified image in Figure 10a is a mosaic of images acquired in December 2004 and February 2005. The velocity map in Figure 10b was produced by correlation of images taken in March 2005 and February 2006. The name of the glacier displayed in Figure 10d is unknown.

divide between the Himalaya to the south and the Tibetan Plateau to the north (Figure 7). The ice-covered areas stretch from the high-relief southern central Himalaya to the low-relief areas on the edge of the Tibetan Plateau to the north, over a horizontal distance of <50 km (Figure 2). Southern glaciers have steep accumulation areas, high percentages of debris-covered areas (34.6 ± 22.8%), and relatively low AARs (0.42 ± 0.26; Figure 7 and Table 1). Conversely, glaciers to the north of the main Himalayan crest have

gentler accumulation areas, lower debris cover (17.9 ± 16), and higher AARs (0.6 ± 0.18).

[37] Measured glacier surface velocities are on average lower than in the Karakoram. In the south, accumulation areas often include steep hillslopes. Ngojumba Glacier, for example, originates on the southern slopes of Cho Oyu peak (8188 m asl) and descends ~1500 m over a horizontal distance of 3.5 km, before it flows another 16 km with an elevation drop of only ~800 m (Figure 9c). Steep icefalls connect

several high-altitude firn fields to the main glacier below. In such places it is difficult to accurately measure velocities or to assess if the ice is flowing at all or simply avalanching. Hence, in this part the interpolated continuous velocity profile that we constructed may not be correct (Figure 9c).

[38] High velocities in the steep upper part of the glaciers contrast with low velocities observed in their gentle sloping lower parts. Changes in velocities farther downstream sometimes occur relatively abruptly although they do not coincide spatially with slope changes, but with the joining of tributary glaciers. Along the profile of Ngojumba Glacier, for example, we note a marked velocity drop at 9–10 km distance from the glacier head at the confluence with the slow moving eastern branch of Ngojumba Glacier (Figures 9a and 9c). A similar phenomenon can be observed at ~8–10 km distance from the head of Rongbuk Glacier (Figure 9d).

[39] Near the terminus, several heavily debris-covered glaciers reach velocities that are within the order of their uncertainties (<2–4 m/yr) [*Quincey et al.*, 2009a; *Scherler et al.*, 2011], and we cannot confidently tell whether the ice is still moving or entirely stagnant (see inset of Figure 9c). Interannual velocity variations are usually much smaller than in the Karakoram and on the order of ~20 m/yr.

4.2.4. Case Study 3: West Kunlun Shan

[40] The total ice-covered areas in the West Kunlun Shan are smaller than in the Karakoram [*von Wissmann*, 1959], but the average fractional ice cover of the catchments is higher (Table 1). Most of the mountain range is covered by a continuous ice surface, which connects north and south flowing glaciers and which is occasionally pierced by nunataks that protrude no more than a few hundred meters above the ice surface. North flowing valley glaciers reach elevations of ~5000 m asl at their termini, whereas the south flowing glaciers are of piedmont type and terminate at ~5500 m asl. Compared to the other study regions, mean catchment relief is lower (0.9 ± 0.2 km), the glaciers have shallower mean surface gradients (12.8 ± 4.3°), large AARs (0.8 ± 0.07) and virtually no debris cover (2.8 ± 2.2%; Figure 7). A notable characteristic in the surface profiles of many glaciers in the West Kunlun Shan is the lack of steep portions in the upper part of the glaciers. Farther downstream, surface slopes are similar to glaciers in other regions, but become steeper toward the glacier terminus.

[41] The pattern of glacier surface velocities in the West Kunlun Shan is unique among all studied regions. Typical velocity profiles are shown in Figure 10. In the upper accumulation area of the glaciers, image correlation is difficult due to permanently snow-covered surfaces with few crevasses or other markers that are suitable for feature tracking. However, the along-flow variations in slope are low, suggesting minor and no abrupt velocity variations. We therefore think that interpolation between limited velocity measurements still provides reasonable results. Despite considerable scatter, the available data suggest generally low velocities that increase approximately linear over the upper two thirds of the profiles. Downstream of the subdued velocity peak, velocities decrease in a parabolic to linear fashion (Figure 10).

[42] Significant interannual variations in flow velocities of up to ~40 m/yr can be observed in the lower parts of the glaciers. Such variability is usually largest (in absolute terms) where velocities are highest and decreases in magnitude upstream and downstream. However, the scarcity of data in the upper part of the glaciers does not allow for accurately deciphering potential variability.

5. Discussion

[43] In the forgone sections we have studied a wide range of glaciers in contrasting landscapes and climates throughout High Asia. Clearly, their dynamics is influenced by many factors, including climate, ice geometry, ice properties, hydrology, and debris cover. It is beyond the scope of this paper to explain all the observed flow behaviors. In the following discussion we intend to highlight some principal observations within a conceptual framework that links the observed glacial dynamics to hillslope processes.

5.1. Topographic Relief, Avalanches, and Debris Cover

[44] The fraction of a glacier surface covered with supraglacial debris mainly depends on the hillslope debris flux relative to the glacier area, and the transport rate and emergence velocity. The hillslope debris flux per unit glacier surface area, in turn is a function of denudation rates and the relative abundance of ice-free hillslopes above the snow line. With our data, we are not able to differentiate between these factors. However, the mean slope angle of all catchment areas above the snow line (ice free and ice covered; Figure 4b) can be regarded as a surrogate for the hillslope debris flux per unit glacier area, as it combines the steepness of ice-free areas with their abundance compared to the low-gradient ice surfaces. The exponential increase of debris cover with mean slope angles is similar to observed increases of erosion rates with mean hillslope angles in ice-free catchments [*Ouimet et al.*, 2009] and may suggest enhanced hillslope debris fluxes at higher slope angles [*Binnie et al.*, 2007]. However, a steeper increase of fractional debris cover with mean slope angles at higher debris cover would be expected even if denudation rates are unchanged, because the melt rate lowering effect of thick debris cover [e.g., *Mattson et al.*, 1993] allows glaciers to grow longer, hence further increasing the percentage of debris-covered areas.

[45] Different hillslope processes can transport debris onto glaciers, but the abrupt increase in debris-covered areas for ice-free hillslope angles >25° suggests that rapid mass movements are more important than diffusive creep processes, which typically dominate at gentler slopes [*Carson and Kirkby*, 1972] (Figure 3). Annually occurring snow avalanches that are thought to initiate at slope angles >25° [*Luckman*, 1977; *Bernhardt and Schulz*, 2010] may actually be important mechanisms that mobilize loose debris from hillslopes [*Rapp*, 1960; *Luckman*, 1977; *Humlum et al.*, 2007]. In periglacial environments, the availability of loose debris mainly depends on the efficacy of frost weathering, and thus a mixture of climatic and lithologic factors [*Walder and Hallet*, 1985; *Hallet et al.*, 1991; *Murton et al.*, 2006; *Hales and Roering*, 2007]. In our analyses, we did not take into account rock type or microclimatic factors, which may explain some of the scatter seen in our data.

[46] We note that during periods of climate warming the degradation of permafrost as well as glacier retreat and debuttressing of hillslopes may lead to an increased frequency of slope failures and thus enhanced flux of debris onto glaciers [e.g., *Church and Slaymaker*, 1989; *Watanabe et al.*, 1998; *Ballantyne*, 2002]. This may temporarily lead

to increased, abnormal debris cover. Although such processes have the potential to deliver large amounts of debris to glaciers during warming periods, we did not observe any massive debris deposits on the studied glaciers that could be related to slope failures during the observation period (2000–2008). Given the large number of satellite images and the 287 studied glaciers, this suggests that nearly continuous high-frequency, low-magnitude events account for most of the observed debris.

5.2. Coupling Hillslope Processes to Glacial Dynamics

[47] When hillslope-derived debris is deposited in the accumulation zone of a glacier, it first becomes englacial during its transport downstream and, at higher concentrations, may reduce the amount of ice deformation [*Russell*, 1895; *Paterson*, 1994] and influence basal sliding [*Iverson et al.*, 2003]. On the glacier surface, however, its main effect is modulating melt rates and thus mass balances. Because debris thicknesses on Himalayan glaciers are usually greater then a few centimeters [e.g., *Shroder et al.*, 2000; *Owen et al.*, 2003; *Heimsath and McGlynn*, 2008], the insulating effect dominates so that melt rates are lower compared to clean ice [*Mattson et al.*, 1993; *Kayastha et al.*, 2000; *Mihalcea et al.*, 2006]. Lower melt rates allow debris-covered glaciers to grow longer for a given accumulation area, hence decreasing the accumulation area ratio (AAR; Figure 3). Because only the ablation zone grows larger, the position of the maximum velocity along a glacier's length, usually located near the ELA or the climatic snow line (Figure 6), should shift upstream as debris cover increases. This inference is supported by our velocity data (Figure 12) and results from a simple numerical model of a debris-covered glacier [*Konrad and Humphrey*, 2000].

[48] When glaciers lie entirely below the present-day snow line (AAR = 0), such as those south of the Nuptse and Lothse peaks in the Khumbu region, central Himalaya (Figure 11), snow accumulation is confined to avalanche depositional areas that are located at the foot of headwalls. In such cases, the climatic snow line is decoupled from the ELA, which is located immediately downstream of the avalanche depositional areas [*Benn and Lehmkuhl*, 2000]. Melt rates in low-lying ablation zones are initially high, especially when the snow and ice are interspersed with dust and debris [*de Scally and Gardner*, 1990]. However, as rapid melting exposes and accumulates the debris on the glacier surface, a continuous debris layer forms and reduces melt rates once its thickness exceeds a few centimeters. Thus, downstream gradients in ice thickness, hence velocity, are steepest in the uppermost part but much gentler in the debris-covered part (Figures 11 and 12).

[49] We note that many Himalayan glaciers have been retreating and/or thinning during the past few decades [e.g., *Berthier et al.*, 2007; *Bolch et al.*, 2008a; *Raina*, 2009], and may have been doing so since ~1850 AD [*Mayewski and Jeschke*, 1979]. This has potential effects on the observed velocity distribution. In particular, heavily debris covered glaciers that are thinning [*Bolch et al.*, 2008a], but not necessarily retreating [*Scherler et al.*, 2011], could result in a gradual shift of maximum velocities upstream and exaggerate the trend we observe. However, the upstream shift of peak velocities with increasing debris cover (Figure 12a) is also observed when excluding stagnating glaciers, suggesting that this is a general trend.

5.3. Glacier Surface Velocities and Erosion Potential

[50] Bedrock abrasion by particles dragged within the ice and glacial quarrying are widely thought to be the most important glacial erosion processes and to depend on basal sliding rates [e.g., *Hallet*, 1979, 1996; *Riihimaki et al.*, 2005; *Amundson and Iverson*, 2006; *Cohen et al.*, 2006]. Although our surface velocities do not allow us to distinguish basal sliding from internal ice deformation, they provide first-order constraints on maximum attainable sliding rates and therefore the downstream distribution of glacial erosion potential. We are aware that there are many other factors which influence the actual erosive work of glaciers, and that certain combinations may even result in fast-flowing glaciers with little erosion potential. However, the flow speed is clearly a limiting factor for both, the erosion and the transport of erosion products, and therefore a useful starting point for a discussion about glacial erosion potential and its relation to hillslope processes.

[51] The altitudinal distribution of velocities, grouped by region, supports the notion of ice flow and thus glacial erosion potential being concentrated at or near the snow line, which closely approximates the ELA for most glaciers [*Brozović et al.*, 1997; *Egholm et al.*, 2009]. Our data also show that the elevation band of highest velocities is lower, by ~0.5 km, in the westerlies-influenced regions as compared to the monsoonal-influenced central Himalaya. Furthermore, in the central Himalaya, glaciers in the northern part have snow lines and concentrated ice flow ~0.5 km higher as compared to southern glaciers. This is most likely related to the Higher Himalaya which acts as a moisture barrier to the Tibetan Plateau [*Ohmura et al.*, 1992]. It is interesting to note that we do not observe such steep north-south gradients in the western regions, which may be related to the higher tropospheric extent of the westerlies, compared to the monsoonal airflow, and deeper penetration of moisture-laden winds into the orogen.

[52] In addition to the downstream and altitudinal distribution of velocities, our data suggest a glacier size dependency of mean surface velocities (Figure 13). However, the range in mean velocities for any given glacier size is high and often spans 1 order of magnitude. For example, similarly extensive glaciers (~10^2 km^2) from the Karakoram and the West Kunlun Shan have mean velocities that vary around ~200 m/yr and ~20 m/yr, respectively (Figure 13a). Such large velocity variations for glaciers of similar size can be related to variations in downstream slope. Following the scaling analysis of the mass and momentum conservation equations by *Bahr et al.* [1997] and *Bahr* [1997], the characteristic glacier downstream velocity is related to the characteristic glacier slope and surface area by a power law. These authors predict scaling exponents of 1.5 for shallow and 1.2 for steep glaciers, when assuming typical flow law parameters and a volume-area scaling exponent of 3/8 (derived from equations (13) and (14) of *Bahr* [1997]). We obtain a scaling exponent of 1.2 ± 0.1 using along-profile means of velocity and slope as characteristic values (R^2 = 0.68; Figure 13b), thus supporting theory and providing confidence in our velocity measurements. In consequence, small
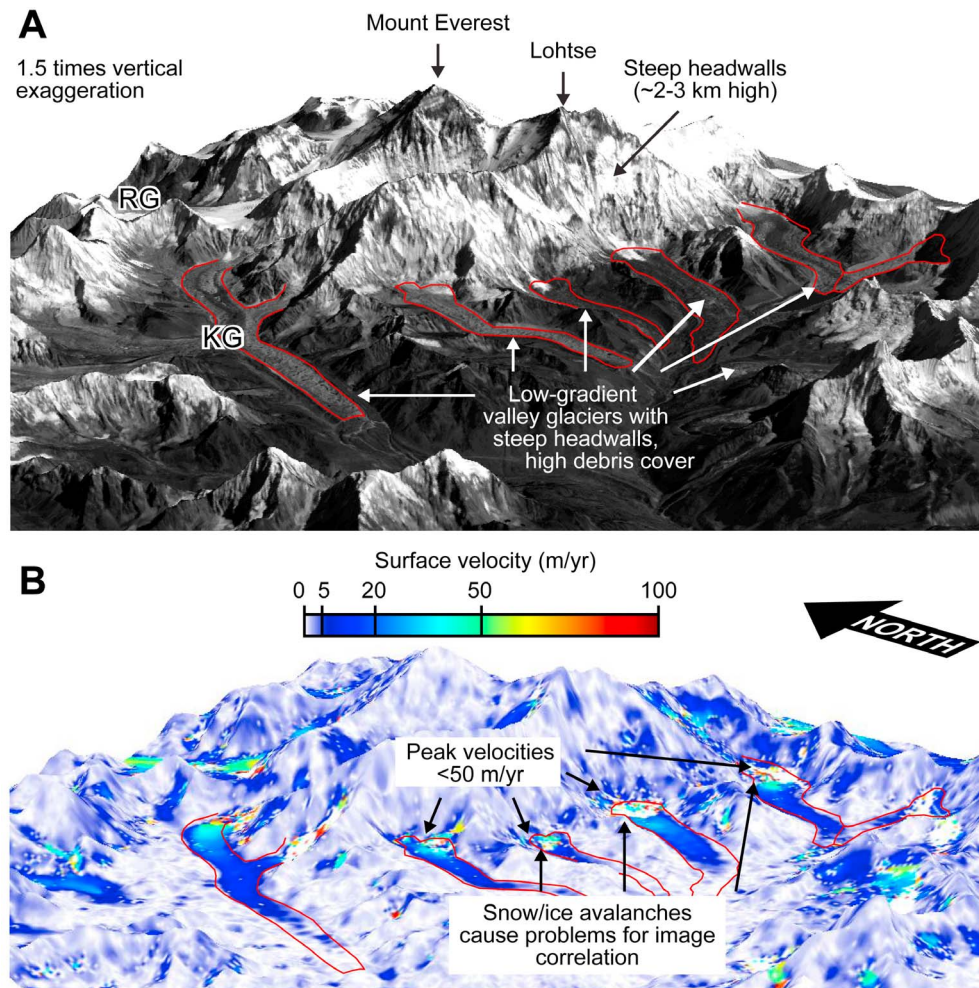
Figure 11. Glacial landscape in the Khumbu Himal, Nepal. (a) Orthorectified ASTER image (band 3N) from 10 November 2004, draped over a 90 m resolution SRTM DEM with 1.5× vertical exaggeration. Accumulation areas are mostly confined to steep and high-reaching headwalls, from where snow and ice avalanches nourish south flowing, low-gradient valley glaciers with high amounts of debris cover located below the snow line. Note lithological contrasts between headwalls (leucogranites) and glacier beds and interfluves (fissile metapelitic gneisses) [*Searle et al.*, 2003]. KG and RG denote Khumbu Glacier and Rongbuk Glacier, respectively. (b) Same view as in Figure 11a but showing mean annual surface velocities between 10 November 2004 and 29 November 2005. Speckled colors at the base of the headwalls indicate miscorrelations, arising from snow and ice avalanches.

but steep glaciers can attain comparable velocities, and thus erosion potential, as long but gentle sloping glaciers, given that the glaciers in question are temperate and no significant differences in the ratio of basal sliding to shear deformation exist. Thus, the size of glaciers alone may in most cases not be sufficient for assessments of their erosion potential [cf. *Berger and Spotila*, 2008].

[53] Finally, in our analysis, we largely omitted surging glaciers, due to insufficient data coverage. Adequately resolving long-term mean velocities of surging glaciers requires velocity measurements that cover a full surge and quiescence cycle, which are so far unavailable. In principle, however, the large velocities that are usually observed during surges have been associated with basal sliding and are therefore tightly linked with the erosion potential. Studies at Variegated Glacier, Alaska, suggest that two thirds of the total erosion during a 20 year surge cycle occurred during a 2 year surge phase

[*Humphrey and Raymond*, 1994]. Because such data are rare, no firm conclusions can be drawn on the general erosion potential of surge-type glaciers. In any case, the advancing fronts of surging glaciers imply that the loci of erosion can propagate to lower elevations as compared to quiescence phases.

5.4. Conceptual Model of Glacial Landscape Development at Plateau Margins

[54] Combining our observations on the coupling of hillslope and glacial processes and the distribution of glacial velocities and erosion potential, we distinguish three different kinds of glacial landscapes in High Asia (Figure 14). These are foremost characterized by differences in topographic relief, which varies from low in the central parts of the Tibetan Plateau to high in the deeply incised mountain ranges along the plateau edges.
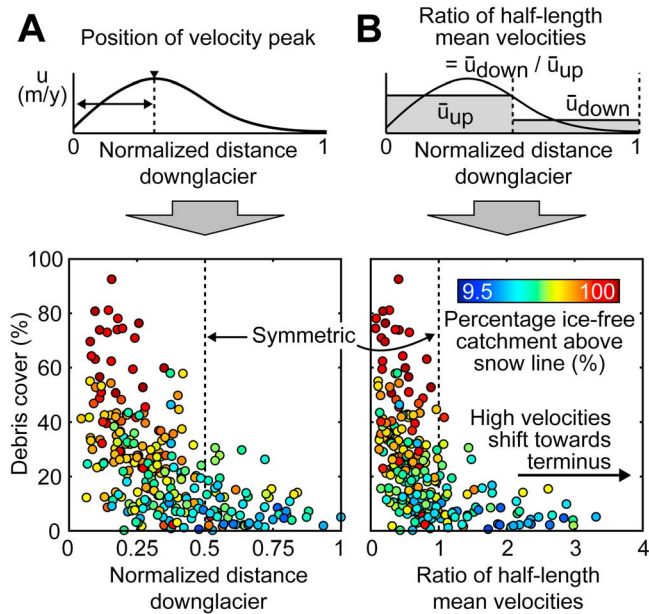
Figure 12. Debris cover and asymmetry of the velocity profiles. (a) Asymmetry of velocity peak versus debris-covered area. The *x* axis shows position of maximum velocity in profile along normalized distance from glacier head. (b) Ratio of half-length mean velocities versus debris-covered area. The *x* axis shows ratio of the mean velocities in the lower to the upper half-lengths of the velocity profiles. In both Figures 12a and 12b, farther left in the plot means that velocities are skewed toward the glacier heads and farther right means that velocities are skewed to the glacier termini. Color coding of data points is a proxy for the degree of snow avalanche contribution to accumulation. See text for details.

[55] Glaciers in low-relief areas, such as the West Kunlun Shan and parts of the northern central Himalaya, have gentle accumulation areas and little or no debris cover, suggesting limited hillslope fluxes (Figure 14a). Due to their shallow gradients, velocities are relatively low and more or less evenly distributed downglacier. Because of their very high elevation, large parts of these glaciers may actually be cold based as indicated by limited borehole measurements [*Liu et al.*, 2009]. In these semiarid to arid environments, melting is observed to be subordinate compared to sublimation [*Ageta et al.*, 1989; *Aizen et al.*, 2002; *Rupper and Roe*, 2008], hence limiting the amount of meltwater, which promotes sliding [*Fountain and Walder*, 1998; *Bartholomaus et al.*, 2008] and therefore erosion [*Iverson*, 1991; *Cohen et al.*, 2006]. These glaciers usually have high AARs, hence small ablation areas, and the part where sliding and erosion probably occurs is therefore near the glacier front, where our data indicate interannual velocity variations that are most likely associated with sliding variations (Figure 10) [e.g., *Willis*, 1995].

[56] Where topography is steeper, an increasing fraction of the accumulation is due to snow and ice avalanching from steep hillslopes. The steeper hillslopes also increase the flux of rocky material to the glaciers and thus their debris covers (Figure 14b). Glaciers that originate from extensive accumulation areas and that descend to low elevations show the highest velocities, particularly at steep segments along their flow path. Such glaciers are probably cold based at higher and temperate at lower elevations [*Shi and Zhang*, 1984]. Karakoram glaciers, for example, show considerable interannual velocity variations in their ablation areas (Figure 8), suggesting high sliding rates [*Quincey et al.*, 2009b] and therefore high erosional potential.

[57] Glaciers that are almost exclusively nourished by snow and ice avalanches have low AARs, the highest amount of supraglacial debris cover and flow velocities are strongly skewed toward their headwalls (Figure 14c). Such glaciers have most areas below the snow line and are likely temperate throughout. However, with gently sloping large debris-mantled parts flowing at low velocities, these glaciers likely have only minor erosion potential along most of their length [*Kääb*, 2005]. Instead, their main erosional and landscape-shaping contribution is the evacuation of hillslope debris, which prevents the formation of scree slopes and ultimately permits continuing headwall retreat.
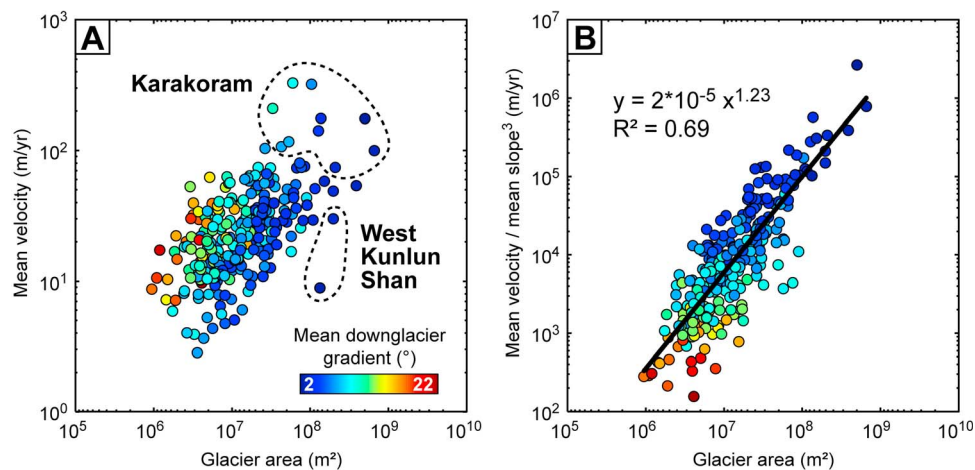

Figure 13. (a) Glacier area versus along-profile mean velocity. Marker colors depict the mean downstream gradient of the glaciers. Note groups of large glaciers with contrasting mean velocities from the Karakoram and the West Kunlun Shan. (b) Glacier area versus along-profile mean velocity divided by mean slope to the power of 3. See text for details.

[58] It is clear that changes in snow line elevations due to climate change or surface uplift modulate the topographic characteristics of glacial accumulation areas and therefore also the hillslope-glacier coupling and the distribution of glacial erosion potential. Considering the case of glacial occupation of a previously ice-free, low-relief continental plateau margin, our conceptual model dictates the transition from a glacier-dominated, low-relief landscape through glacial incision toward a high-relief landscape in which periglacial hillslope processes become more important in lowering topography (Figure 15). If no rock uplift occurs, glacial and hillslope erosion ultimately result in shrinking accumulation areas and thus glacier recession, as is typically observed in numerical models of glacial erosion [e.g., *Egholm et al.*, 2009; *MacGregor et al.*, 2009].

Figure 15. Conceptual sketch showing the morphologic evolution of a plateau-like landscape under glacial influence. Incipient glaciation (A) is mostly cold based and little erosive. Progressive glacial downcutting, starting at the lower end of glaciers, increases relief and thus hillslope fluxes (B). Eventually, steep accumulation areas account for significant headwall retreat, but glaciers that are located mostly below the snow line have little erosion potential and mostly act as debris conveyors (C). Depending on climate and rock uplift rates, glaciers and hillslopes may maintain higher or lower erosion rates.

[59] We note that in our conceptual model, glacial erosion is producing relief whereas headwall retreat, achieved through periglacial weathering and efficient hillslope clearing by rockfalls, snow and ice avalanches, is reducing relief. During this stage, the rate of headwall retreat is related to periglacial weathering rates rather than glacial erosion rates [*Hales and Roering*, 2005], while the glaciers act mainly as debris conveyors. Thus, when relating this to a buzz saw mechanism that limits topographic growth at or near the snow line [*Brozović et al.*, 1997; *Egholm et al.*, 2009], periglacial processes may be more important for beveling of topography as compared to glaciers, which set the base level for the hillslopes.

6. Conclusions

[60] We have presented a synthesis of the coupling between hillslopes and glacial flow behavior in High Asia. In these complex landscapes, the interplay of climate and topography sets the boundary conditions for the development of different glacier types, sizes, and geometries, which are all first-order controls on their flow speeds. Our data show how the downstream distribution of glacier velocities is further affected by the presence of debris cover, which is a function of the steepness of the accumulation areas. Maximum glacial velocities are progressively shifted upglacier as accumulation areas get steeper and hillslope debris fluxes increase. This is what we refer to as hillslope-glacier coupling.

[61] The coupling of hillslope processes and glacial dynamics increases with the areal fraction of debris cover to the point where heavily debris covered glaciers that are located below the snow line and are fed entirely by avalanches, may only act as debris conveyors. These help to clear
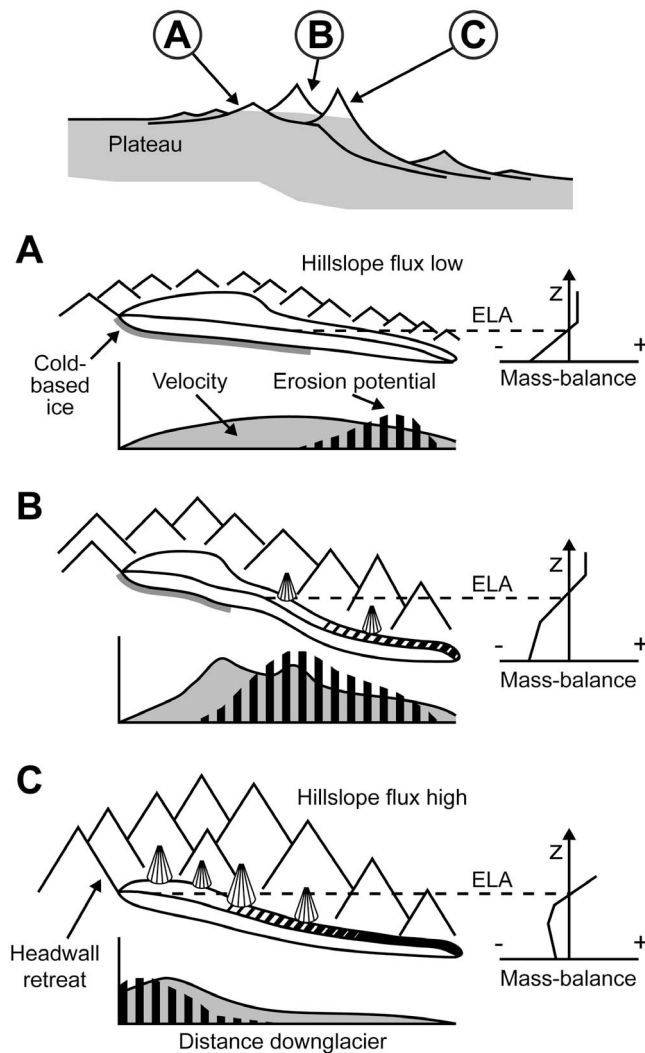

Figure 14. Schematic effect of topography on accumulation types, debris covers, glacier flow velocities, and erosion potentials in High Asia. (a) Mostly cold-based glacier in a low-relief landscape, which is dominantly fed by direct snowfall and which has no debris cover (e.g., West Kunlun Shan). (b) Polythermal glacier fed by both avalanches and direct snowfall (e.g., Karakoram, western Himalaya). (c) Temperate glacier dominantly fed by avalanches and with abundant debris cover (e.g., southern central Himalaya).
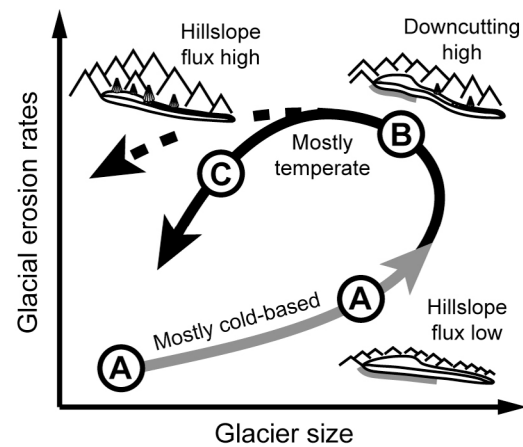
off the base of headwalls, and thus prevent the formation of scree slopes and thereby allow continued headwall retreat, but have little erosion potential. The continuum of low- to high-relief glacial landscapes on the Tibetan Plateau and its margins can be conceptualized by sequential stages during the glacial modification of a low-relief plateau margin landscape. As glaciers cut down and steepen their catchments, periglacial hillslope processes gain geomorphic relevance and eventually feed back on the glacial dynamics.

[62] In this study, we have restricted our focus on the flux of material from the hillslopes and its transport by the glaciers. Glaciers deposit this material in form of moraines, which are used to reconstruct glacial extents. In this respect, the histories of erratic boulders on moraines may be quite different in landscapes of different relief. We therefore suggest that differences in glacial dynamics that are associated with contrasting topographic settings need to be considered when inferring past glacial episodes from dated moraines [e.g., *Owen et al.*, 2008; *Scherler et al.*, 2010]. In particular, correlating glacial chronologies between areas with strikingly different relief characteristics may lead to misinterpretations. Differences in glacier dynamics are also manifested on shorter time scales and need to be considered when studying the response of glaciers to recent climate change [e.g., *Scherler et al.*, 2011].

References

Ageta, Y., and K. Higuchi (1984), Estimation of mass balance components of a summer-accumulation type glacier in the Nepal Himalaya, *Geogr. Ann., Ser. A, Phys. Geogr.*, 66, 249–255, doi:10.2307/520698.

Ageta, Y., W. Zhang, and M. Nakawo (1989), Mass balance studies on Chongce Ice Cap in the West Kunlun Mountains, *Bull. Glacier Res.*, 7, 37–43.

Aizen, V. B., E. M. Aizen, and V. N. Nikitin (2002), Glacier regime on the northern slope of the Himalaya (Xixibangma glaciers), *Quat. Int.*, 97–98, 27–39, doi:10.1016/S1040-6182(02)00049-6.

Amundson, J. M., and N. R. Iverson (2006), Testing a glacial erosion rule using hang heights of hanging valleys, Jasper National Park, Alberta, Canada, *J. Geophys. Res.*, 111, F01020, doi:10.1029/2005JF000359.

Anders, A. M., G. H. Roe, B. Hallet, D. R. Montgomery, N. J. Finnegan, and J. Putkonen (2006), Spatial patterns of precipitation and topography in the Himalaya, in *Tectonics, Climate, and Landscape Evolution*, edited by S. D. Willett et al., *Spec. Pap. Geol. Soc. Am.*, 398, 39–53, doi:10.1130/2006.2398(03).

Anderson, R. S. (2005), Teflon peaks: The evolution of high local relief in glaciated mountain ranges, *Eos Trans. AGU*, 86(52), Fall Meet. Suppl., Abstract H33F-04.

Anderson, R. S., P. Molnar, and M. A. Kessler (2006), Features of glacial valley profiles simply explained, *J. Geophys. Res.*, 111, F01004, doi:10.1029/2005JF000344.

Avouac, J.-P., F. Ayoub, S. Leprince, O. Konca, and D. V. Helmberger (2006), The 2005, Mw 7.6 Kashmir earthquake: Sub-pixel correlation of ASTER images and seismic waveform analysis, *Earth Planet. Sci. Lett.*, 249(3–4), 514–528, doi:10.1016/j.epsl.2006.06.025.

Bahr, D. B. (1997), Global distributions of glacier properties: A stochastic scaling paradigm, *Water Resour. Res.*, 33(7), 1669–1679, doi:10.1029/97WR00824.

Bahr, D. B., M. F. Meier, and S. D. Peckham (1997), The physical basis of glacier volume-area scaling, *J. Geophys. Res.*, 102(B9), 20,355–20,362, doi:10.1029/97JB01696.

Ballantyne, C. K. (2002), Paraglacial geomorphology, *Quat. Sci. Rev.*, 21, 1935–2017, doi:10.1016/S0277-3791(02)00005-7.

Barry, R. G., and R. J. Chorley (2003), *Atmosphere, Weather and Climate*, 472 pp., Routledge, London.

Bartholomaus, T. C., R. S. Anderson, and S. P. Anderson (2008), Response of glacier basal motion to transient water storage, *Nat. Geosci.*, 1, 33–37, doi:10.1038/ngeo.2007.52.

Benn, D. I., and F. Lehmkuhl (2000), Mass balance and equilibrium-line altitudes of glaciers in high-mountain environments, *Quat. Int.*, 65–66, 15–29, doi:10.1016/S1040-6182(99)00034-8.

Benn, D. I., and L. A. Owen (1998), The role of the Indian summer monsoon and the midlatitude westerlies in Himalayan glaciation: Review and speculative discussion, *J. Geol. Soc.*, 155, 353–363, doi:10.1144/gsjgs.155.2.0353.

Berger, A. L., and J. A. Spotila (2008), Denudation and deformation in a glaciated orogenic wedge: The St. Elias orogen, Alaska, *Geology*, 36(7), 523–526, doi:10.1130/G24883A.1.

Bernhardt, M., and K. Schulz (2010), SnowSlide: A simple routine for calculating gravitational snow transport, *Geophys. Res. Lett.*, 37, L11502, doi:10.1029/2010GL043086.

Berthier, E., H. Vadon, D. Baratoux, Y. Arnaud, C. Vincent, K. L. Feigl, F. Rémy, and B. Legrésy (2005), Surface motion of mountain glaciers derived from satellite optical imagery, *Remote Sens. Environ.*, 95, 14–28, doi:10.1016/j.rse.2004.11.005.

Berthier, E., Y. Arnaud, R. Kumar, S. Ahmad, P. Wagnon, and P. Chevallier (2007), Remote sensing estimates of glacier mass balances in the Himachal Pradesh (western Himalaya, India), *Remote Sens. Environ.*, 108, 327–338, doi:10.1016/j.rse.2006.11.017.

Bhutiyani, M. R. (1999), Mass-balance studies on Siachen Glacier in the Nubra valley, Karakoram Himalaya, India, *J. Glaciol.*, 45(149), 112–118.

Binnie, S. A., W. M. Phillips, M. A. Summerfield, and L. K. Fifield (2007), Tectonic uplift, threshold hillslopes, and denudation rates in a developing mountain range, *Geology*, 35(8), 743–746, doi:10.1130/G23641A.1.

Bolch, T., M. Buchroithner, T. Pieczonka, and A. Kunert (2008a), Planimetric and volumetric glacier changes in the Khumbu Himal, Nepal, since 1962 using Corona, Landsat TM and ASTER data, *J. Glaciol.*, 54(187), 592–600, doi:10.3189/002214308786570782.

Bookhagen, B., and D. W. Burbank (2006), Topography, relief, and TRMM-derived rainfall variations along the Himalaya, *Geophys. Res. Lett.*, 33, L08405, doi:10.1029/2006GL026037.

Bookhagen, B., and D. W. Burbank (2010), Toward a complete Himalayan hydrologic budget: Spatiotemporal distribution of snowmelt and rainfall and their impact on river discharge, *J. Geophys. Res.*, 115, F03019, doi:10.1029/2009JF001426.

Boos, W. R., and Z. Kuang (2010), Dominant control of the South Asian monsoon by orographic insulation versus plateau heating, *Nature*, 463, 218–222, doi:10.1038/nature08707.

Boulton, G. S., and N. Eyles (1979), Sedimentation by valley glaciers: A model and genetic classification, in *Moraines and Varves*, edited by C. Schluchter, pp. 11–23, A. A. Balkema, Rotterdam, Netherlands.

Brocklehurst, S. H., and K. X. Whipple (2007), Response of glacial landscapes to spatial variations in rock uplift rate, *J. Geophys. Res.*, 112, F02035, doi:10.1029/2006JF000667.

Brozović, N., D. W. Burbank, and A. J. Meigs (1997), Climatic limits on landscape development in the northwestern Himalaya, *Science*, 276, 571–574, doi:10.1126/science.276.5312.571.

Burbank, D. W., A. E. Blythe, J. Putkonen, B. Pratt-Sitaula, E. Gabet, M. Oskin, A. Barros, and T. P. Ojha (2003), Decoupling of erosion and precipitation in the Himalayas, *Nature*, 426, 652–655, doi:10.1038/nature02187.

Carson, M. A., and M. J. Kirkby (1972), *Hillslope Form and Process*, 475 pp., Cambridge Univ. Press, Cambridge, U. K.

Church, M., and O. Slaymaker (1989), Disequilibrium of Holocene sediment yield in glaciated British Columbia, *Nature*, 337, 452–454, doi:10.1038/337452a0.

Clayton, L. (1964), Karst topography on stagnant glaciers, *J. Glaciol.*, 5(37), 107–112.

Cohen, D., T. S. Hooyer, N. R. Iverson, J. F. Thomason, and M. Jackson (2006), Role of transient water pressure in quarrying: A subglacial experiment using acoustic emissions, *J. Geophys. Res.*, 111, F03006, doi:10.1029/2005JF000439.

de Scally, F. A., and J. F. Gardner (1990), Ablation of avalanched and undisturbed snow, Himalaya mountains, Pakistan, *Water Resour. Res.*, 26(11), 2757–2767.

Dyurgerov, M. B., and M. F. Meier (2005), Glaciers and the changing Earth system: A 2004 snapshot, *Occas. Pap. 58*, 118 pp., Inst. of Arctic and Alp. Res., Univ. of Colo. at Boulder, Boulder. [Available at http://instaar.colorado.edu/other/download/OP58_dyurgerov_meier.pdf]

Egholm, D. L., S. B. Nielsen, V. K. Pedersen, and J.-E. Lesemann (2009), Glacial effects limiting mountain height, *Nat. Geosci.*, 460, 884–887, doi:10.1038/nature08263.

Farr, T. G., et al. (2007), The Shuttle Radar Topography Mission, *Rev. Geophys.*, 45, RG2004, doi:10.1029/2005RG000183.

Fountain, A. G., and J. S. Walder (1998), Water flow through temperate glaciers, *Rev. Geophys.*, 36(3), 299–328, doi:10.1029/97RG03579.

Gabet, E. J., D. W. Burbank, B. Pratt-Sitaula, J. Putkonen, and B. Bookhagen (2008), Modern erosion rates in the high Himalayas of Nepal, *Earth Planet. Sci. Lett.*, 267(3–4), 482–494, doi:10.1016/j.epsl.2007.11.059.

Hahn, D. G., and S. Manabe (1975), The role of mountains in the South Asian monsoon circulation, *J. Atmos. Sci.*, 32, 1515–1541, doi:10.1175/1520-0469(1975)032<1515:TROMIT>2.0.CO;2.

Hales, T. C., and J. J. Roering (2005), Climate-controlled variations in scree production, Southern Alps, New Zealand, *Geology*, 33(9), 701–704, doi:10.1130/G21528.1.

Hales, T. C., and J. J. Roering (2007), Climatic controls on frost cracking and implications for the evolution of bedrock landscapes, *J. Geophys. Res.*, 112, F02033, doi:10.1029/2006JF000616.

Hallet, B. (1979), A theoretical model of glacial abrasion, *J. Glaciol.*, 23(89), 39–50.

Hallet, B. (1996), Glacial quarrying: A simple theoretical model, *Ann. Glaciol.*, 22, 1–8.

Hallet, B., J. S. Walder, and C. W. Stubbs (1991), Weathering by segregation ice growth in microcracks at sustained subzero temperatures: Verification from an experimental study using acoustic emissions, *Arct. Alp. Res.*, 2, 283–300.

Harper, J. T., and N. F. Humphrey (2003), High altitude Himalayan climate inferred from glacial ice flux, *Geophys. Res. Lett.*, 30(14), 1764, doi:10.1029/2003GL017329.

Heimsath, A. M., and R. S. McGlynn (2008), Quantifying headwall retreat rates in the Nepal high Himalaya, *Geomorphology*, 97(1–2), 5–23, doi:10.1016/j.geomorph.2007.02.046.

Hewitt, K. (2007), Tributary glacier surges: An exceptional concentration at Panmah Glacier, Karakoram Himalaya, *J. Glaciol.*, 53(181), 181–188, doi:10.3189/172756507782202829.

Hewitt, K. (2009), Catastrophic rock slope failures and late Quaternary developments in the Nanga Parbat-Haramosh Massif, Upper Indus basin, northern Pakistan, *Quat. Sci. Rev.*, 28, 1055–1069, doi:10.1016/j.quascirev.2008.12.019.

Humlum, O., H. H. Christiansen, and H. Juliussen (2007), Avalanche-derived rock glaciers in Svalbard, *Permafrost Periglacial Processes*, 18(1), 75–88, doi:10.1002/ppp.580.

Humphrey, N. F., and C. F. Raymond (1994), Hydrology, erosion, and sediment production in a surging glacier: Variegated Glacier, Alaska, 1982–1983, *J. Glaciol.*, 40(136), 539–552.

Inoue, J. (1977), Mass budget of Khumbu Glacier, *Seppyo*, 39, 15–19.

Iverson, N. R. (1991), Potential effects of subglacial water-pressure fluctuations on quarrying, *J. Glaciol.*, 37(125), 27–36.

Iverson, N. R., D. Cohen, T. S. Hooyer, U. H. Fischer, M. Jackson, P. L. Moore, G. Lappegard, and J. Kohler (2003), Effects of basal debris on glacier flow, *Science*, 301, 81–84, doi:10.1126/science.1083086.

Jóhannesson, T., C. F. Raymond, and E. D. Vaddington (1989), A simple method for determining the response time of glaciers, in *Glacier Oscillations and Climatic Change*, edited by J. Oeriemans, pp. 343–352, Kluwer Acad., Dordrecht, Netherlands.

Kääb, A. (2005), Combination of SRTM3 and repeat ASTER data for deriving alpine glacier flow velocities in the Bhutan Himalaya, *Remote Sens. Environ.*, 94, 463–474, doi:10.1016/j.rse.2004.11.003.

Kargel, J. S., et al. (2005), Multispectral imaging contributions to global land ice measurements from space, *Remote Sens. Environ.*, 99, 187–219, doi:10.1016/j.rse.2005.07.004.

Kayastha, R. B., Y. Takeuchi, M. Nakawo, and Y. Ageta (2000), Practical prediction of ice melting beneath various thickness of debris cover on Khumbu Glacier, Nepal, using a positive degree-day factor, in *Debris-Covered Glaciers*, edited by M. Nakawo, C. F. Raymond, and A. Fountain, *IAHS Publ.*, 264, 71–82.

Kirkbride, M. P. (1993), The temporal significance of transitions from melting to calving termini at glaciers in the central Southern Alps of New Zealand, *Holocene*, 3(3), 232–240, doi:10.1177/095968369300300305.

Konrad, S. K., and N. F. Humphrey (2000), Steady-state flow model of debris-covered glaciers (rock glaciers), in *Debris-Covered Glaciers*,

edited by M. Nakawo, C. F. Raymond, and A. Fountain, *IAHS Publ.*, 264, 255–263.

Leprince, S., S. Barbot, F. Ayoub, and J.-P. Avouac (2007), Automatic and precise orthorectification, coregistration, and subpixel correlation of satellite images, application to ground deformation measurements, *IEEE Trans. Geosci. Remote Sens.*, 45(6), 1529–1558, doi:10.1109/TGRS.2006.888937.

Leprince, S., E. Berthier, F. Ayoub, C. Delacourt, and J.-P. Avouac (2008), Monitoring Earth surface dynamics with optical imagery, *Eos Trans. AGU*, 89(1), 1, doi:10.1029/2008EO010001.

Liu, Y., S. Hou, Y. Wang, and L. Song (2009), Distribution of borehole temperature at four high-altitude alpine glaciers in central Asia, *J. Mt. Sci.*, 6, 221–227.

Luckman, B. H. (1977), The geomorphic activity of snow avalanches, *Geogr. Ann., Ser. A, Phys. Geogr.*, 59, 31–48, doi:10.2307/520580.

MacGregor, K. R., R. S. Anderson, and E. D. Waddington (2009), Numerical modeling of glacial erosion and headwall processes in alpine valleys, *Geomorphology*, 103(2), 189–204, doi:10.1016/j.geomorph.2008.04.022.

Mattson, L. E., J. S. Gardner, and G. J. Young (1993), Ablation on debris covered glaciers: An example from the Rakhiot Glacier, Punjab, Himalaya, in *Snow and Glacier Hydrology*, edited by G. J. Young, *IAHS Publ.*, 218, 289–296.

Mayewski, P. A., and P. A. Jeschke (1979), Himalayan and trans-Himalayan glacier fluctuations since AD 1812, *Arct. Alp. Res.*, 11(3), 267–287, doi:10.2307/1550417.

Meier, M. F., and A. S. Post (1962), Recent variations in mass net budgets of glaciers in western North America, *Int. Assoc. Sci. Hydrol. Publ.*, 58, 63–77.

Mihalcea, C., C. Myer, G. Diolaiuti, A. Lambrecht, C. Smiraglia, and G. Tartari (2006), Ice ablation and meteorological conditions on the debris-covered area of Baltoro Glacier, Karakoram, Pakistan, *Ann. Glaciol.*, 43, 292–300, doi:10.3189/172756406781812104.

Mitchell, S. G., and D. R. Montgomery (2006), Influence of a glacial buzz-saw on the height and morphology of the Washington Cascade Range, Washington State, USA, *Quat. Res.*, 65(1), 96–107, doi:10.1016/j.yqres.2005.08.018.

Murton, J. B., R. Peterson, and J.-C. Ozouf (2006), Bedrock fracture by ice segregation in cold regions, *Science*, 314, 1127–1129, doi:10.1126/science.1132127.

Naylor, S., and E. J. Gabet (2007), Valley asymmetry and glacial versus nonglacial erosion in the Bitterroot Range, Montana, USA, *Geology*, 35(4), 375–378, doi:10.1130/G23283A.1.

O'Callaghan, J. F., and D. M. Mark (1984), The extraction of drainage networks from digital elevation data, *Comput. Vis. Graph. Image Process.*, 28, 323–344, doi:10.1016/S0734-189X(84)80011-0.

Ogilvie, I. H. (1904), The effect of superglacial debris on the advance and retreat of some Canadian glaciers, *J. Geol.*, 12(8), 722–743, doi:10.1086/621194.

Ohata, T., S. Takahashi, and X. Kang (1989), Meteorological conditions of the West Kunlun Mountains in the summer of 1987, *Bull. Glacier Res.*, 7, 67–76.

Ohmura, A., P. Kasser, and M. Funk (1992), Climate at the equilibrium line of glaciers, *J. Glaciol.*, 38(130), 397–411.

Oskin, M., and D. W. Burbank (2005), Alpine landscape evolution dominated by cirque retreat, *Geology*, 33(12), 933–936, doi:10.1130/G21957.1.

Osmaston, H. (2005), Estimates of glacier equilibrium line altitudes by the area × altitude, the area × altitude balance ratio and the area × altitude balance index methods and their validation, *Quat. Int.*, 138–139, 22–31, doi:10.1016/j.quaint.2005.02.004.

Østrem, G. (1959), Ice melting under a thin layer of moraine, and the existence of ice cores in moraine ridges, *Geogr. Ann.*, 41, 228–230.

Ouimet, W. B., K. X. Whipple, and D. E. Granger (2009), Beyond threshold hillslopes: Channel adjustment to base-level fall in tectonically active mountain ranges, *Geology*, 37(7), 579–582, doi:10.1130/G30013A.1.

Owen, L. A., E. Derbyshire, and C. H. Scott (2003), Contemporary sediment production and transfer in high-altitude glaciers, *Sediment. Geol.*, 155, 13–36, doi:10.1016/S0037-0738(02)00156-2.

Owen, L. A., M. W. Caffee, R. C. Finkel, and B. Y. Seong (2008), Quaternary glaciations of the Himalayan-Tibetan orogen, *J. Quat. Sci.*, 23, 513–531, doi:10.1002/jqs.1203.

Paterson, W. S. B. (1994), *The Physics of Glaciers*, 480 pp., Elsevier, New York.

Paul, F., C. Huggel, and A. Kääb (2004), Combining satellite multispectral image data and a digital elevation model for mapping debris-covered glaciers, *Remote Sens. Environ.*, 89, 510–518, doi:10.1016/j.rse.2003.11.007.

Pedersen, V. K., D. L. Egholm, and S. B. Nielsen (2010), Alpine glacial topography and the rate of rock column uplift: A global perspective, *Geomorphology*, *122*(1–2), 129–139, doi:10.1016/j.geomorph.2010.06.005.

Quincey, D. J., A. Luckman, and D. I. Benn (2009a), Quantification of Everest region glacier velocities between 1992 and 2002, using satellite radar interferometry and feature tracking, *J. Glaciol.*, *55*(192), 596–606, doi:10.3189/002214309789470987.

Quincey, D. J., L. Copland, C. Mayer, M. Bishop, A. Luckman, and M. Beló (2009b), Ice velocity and climate variations for Baltoro Glacier, Pakistan, *J. Glaciol.*, *55*(194), 1061–1071, doi:10.3189/002214309790794913.

Rabatel, A., J.-P. Dedieu, and C. Vincent (2005), Using remote-sensing data to determine equilibrium-line altitude and mass-balance time series: Validation on three French glaciers, 1994–2002, *J. Glaciol.*, *51*(175), 539–546, doi:10.3189/172756505781829106.

Raina, V. K. (2009), Himalayan glaciers: A state-of-art review of glacial studies, glacial retreat and climate change, discussion paper, 60 pp., Minist. of Environ. and For., New Delhi. [Available at http://moef.nic. in/downloads/public-information/MoEF%20Discussion%20Paper%20_ him.pdf.]

Rapp, A. (1960), Recent development of mountain slopes in Karkevagge and surroundings, northern Scandinavia, *Geogr. Ann.*, *42*, 65–200, doi:10.2307/520126.

Riihimaki, C. A., K. R. MacGregor, R. S. Anderson, S. P. Anderson, and M. G. Loso (2005), Sediment evacuation and glacial erosion rates at a small alpine glacier, *J. Geophys. Res.*, *110*, F03003, doi:10.1029/ 2004JF000189.

Rupper, S., and G. Roe (2008), Glacier changes and regional climate: A mass and energy balance approach, *J. Clim.*, *21*, 5384–5401, doi:10.1175/2008JCLI2219.1.

Russell, I. C. (1895), The influence of debris on the flow of glaciers, *J. Geol.*, *3*(7), 823–832, doi:10.1086/607340.

Scambos, T. A., M. J. Dutkiewicz, J. C. Wilson, and R. A. Bindschadler (1992), Application of image cross-correlation to the measurement of glacier velocity using satellite image data, *Remote Sens. Environ.*, *42*, 177–186, doi:10.1016/0034-4257(92)90101-O.

Scherler, D., S. Leprince, and M. R. Strecker (2008), Glacier-surface velocities in alpine terrain from optical satellite imagery—Accuracy improvement and quality assessment, *Remote Sens. Environ.*, *112*, 3806–3819, doi:10.1016/j.rse.2008.05.018.

Scherler, D., B. Bookhagen, M. R. Strecker, F. von Blanckenburg, and D. Rood (2010), Timing and extent of late Quaternary glaciation in the western Himalaya constrained by [10]Be moraine dating in Garhwal, India, *Quat. Sci. Rev.*, *29*, 815–831, doi:10.1016/j.quascirev.2009.11.031.

Scherler, D., B. Bookhagen, and M. R. Strecker (2011), Spatially variable response of Himalayan glaciers to climate change affected by debris cover, *Nat. Geosci.*, doi:10.1038/ngeo1068.

Schlagintweit, H. (1871), *Reisen in Indien und Hochasien*, vol. 2, *Hochasien 1: Der Himálaya von Bhután bis Kashmir*, 468 pp., Costenoble, Gotha, Germany.

Searle, M. P., R. L Simpson, R. D. Law, R. R. Parrish, and D. J. Waters (2003), The structural geometry, metamorphic and magmatic evolution of the Everest massif, High Himalaya of Nepal-South Tibet, *J. Geol. Soc. London*, *160*, 345–366.

Shi, Y., and X. Zhang (1984), Some studies of the Batura glacier in the Karakoram Mountains, in *The International Karakoram Project*, vol. 1, edited by K. J. Miller, pp. 51–63, Cambridge Univ. Press, Cambridge, U. K.

Shroder, J. F., M. P. Bishop, L. Copland, and V. F. Sloan (2000), Debris-covered glaciers and rock glaciers in the Nanga Parbat Himalaya, Pakistan, *Geogr. Ann., Ser. A, Phys. Geogr.*, *82*, 17–31, doi:10.1111/ j.0435-3676.2000.00108.x.

Spotila, J. A., J. T. Buscher, A. J. Meigs, and P. W. Reiners (2004), Long-term glacial erosion of active mountain belts: Example of the Chugach-St. Elias Range, Alaska, *Geology*, *32*(6), 501–504, doi:10.1130/ G20343.1.

van der Beek, P., J. Van Melle, S. Guillot, A. Pêcher, P. W. Reiners, S. Nicolescu, and M. Latif (2009), Eocene Tibetan plateau remnants preserved in the northwest Himalaya, *Nat. Geosci.*, *2*, 364–368, doi:10.1038/ngeo503.

von Wissmann, H. (1959), Die heutige Vergletscherung und Schneegrenze in Hochasien mit Hinweisen auf die Vergletscherung der letzten Eiszeit, *Abh. Math. Naturwiss. Kl. Akad. Wiss. Lit. Mainz*, *14*, 1101–1431.

Walder, J., and B. Hallet (1985), A theoretical model of the fracture of rock during freezing, *Geol. Soc. Am. Bull.*, *96*, 336–346, doi:10.1130/0016-7606(1985)96<336:ATMOTF>2.0.CO;2.

Watanabe, T., L. Dali, and T. Shiraiwa (1998), Slope denudation and the supply of debris to cones in Langtang Himal, central Nepal Himalaya, *Geomorphology*, *26*(1–3), 185–197, doi:10.1016/S0169-555X(98) 00058-0.

Weiers, S. (1994), *Zur Klimatologie des NW-Karakoram und Angrenzender Gebiete*, vol. 92, 169 pp., Bonner Geogr. Abh., Bonn, Germany.

Willis, I. C. (1995), Intra-annual variations in glacier motion: A review, *Prog. Phys. Geogr.*, *19*(1), 61–106, doi:10.1177/030913339501900104.

Winiger, M., M. Gumpert, and H. Yamout (2005), Karakorum-Hindukush-western Himalaya, assessing high-altitude water resources, *Hydrol. Processes*, *19*, 2329–2338, doi:10.1002/hyp.5887.

Wulf, H., B. Bookhagen, and D. Scherler (2010), Seasonal precipitation gradients and their impact on fluvial sediment flux in the northwest Himalaya, *Geomorphology*, *118*(1–2), 13–21, doi:10.1016/j.geomorph. 2009.12.003.

B. Bookhagen, Department of Geography, University of California, 1832 Ellison Hall, Santa Barbara, CA 93106-4060, USA.

D. Scherler and M. R. Strecker, Institut für Geowissenschaften, Universität Potsdam, Karl-Liebknecht-Str. 24, D-14476 Potsdam, Germany. (dirk@geo.uni-potsdam.de)